

# On the Use of Blanketed Atmospheres as Boundary Conditions for Stellar Evolutionary Models

Don A. Vandenberg

*Department of Physics & Astronomy, University of Victoria, P.O. Box 3055, Victoria,  
B.C., V8W 3P6, Canada*

vandenbe@uvic.ca

Bengt Edvardsson

*Uppsala Astronomical Observatory, Box 515, SE-751 20 Uppsala, Sweden*

be@astro.uu.se

Kjell Eriksson

*Uppsala Astronomical Observatory, Box 515, SE-751 20 Uppsala, Sweden*

Kjell.Eriksson@astro.uu.se

Bengt Gustafsson

*Uppsala Astronomical Observatory, Box 515, SE-751 20 Uppsala, Sweden*

bg@astro.uu.se

## ABSTRACT

Stellar models have been computed for stars having  $[\text{Fe}/\text{H}] = 0.0$  and  $-2.0$  to determine the effects, primarily on the predicted  $T_{\text{eff}}$  scale, of using boundary conditions derived from the latest MARCS model atmospheres. The latter have been fitted to the interior models at both the photosphere and at  $\tau = 100$ , and, at least for the  $0.8\text{--}1.0M_{\odot}$  stars considered here, the resultant evolutionary tracks on the H-R diagram were found to be nearly independent of the chosen fitting point. Particular care was taken to treat the entire star as consistently as possible; i.e., both the stellar structure and atmosphere codes assumed the same abundances of helium and the heavy elements, as well as the same treatment of convection (the mixing-length theory, with the free parameter  $\alpha_{\text{MLT}}$  chosen to satisfy the solar constraint). Tracks were also computed in which the photospheric pressure was

obtained by integrating the hydrostatic equation together with either the classical gray  $T(\tau, T_{\text{eff}})$  relation or that derived by Krishna Swamy (1966) from an empirical solar atmosphere. Due to the compensating effects of differences in the calibrated values of  $\alpha_{\text{MLT}}$ , the evolutionary sequences that assumed gray atmospheric structures were in fortuitously close agreement with those using MARCS atmospheres as boundary conditions, independently of the assumed metallicity. (The structures of gray atmospheres are quite different from those predicted by MARCS models.) On the other hand, the models based on the Krishna Swamy  $T(\tau, T_{\text{eff}})$  relationship implied a much hotter giant branch (by  $\sim 150$  K) at solar abundances, which happens to be in good agreement with the inferred temperatures of giants in the open cluster M 67 from the latest  $(V - K) - T_{\text{eff}}$  relations, though they were similar to the other cases at  $[\text{Fe}/\text{H}] = -2.0$ . Most of the computations assumed  $Z = 0.0125$  for the Sun, as derived by M. Asplund and colleagues, though a few models were calculated for  $Z = 0.0165$ , assuming the Grevesse & Sauval (1998) metals mix, to determine the dependence of the evolutionary tracks on  $Z_{\odot}$ . Grids of “scaled solar, differentially corrected” (SDC) atmospheres were also computed, to try to improve upon theoretical MARCS models. When they were used to describe the surface layers of stellar models, the resultant tracks were in remarkably good agreement with those that employed a standard scaled-solar (e.g., Krishna Swamy)  $T(\tau, T_{\text{eff}})$  relation to derive the boundary pressures, independently of the assumed metal abundance. To within current distance and metallicity uncertainties, it was possible to obtain a good match of isochrones for  $[\text{Fe}/\text{H}] = -2.0$  to the C-M diagram of the globular cluster M 68. Until these uncertainties and those associated with the atmospheric boundary conditions are reduced significantly, it cannot be claimed with any confidence that  $\alpha_{\text{MLT}}$  does or does not vary with  $[\text{Fe}/\text{H}]$ . While our consideration of M 67 giants suggests that this parameter is independent of  $T_{\text{eff}}$  and  $\log g$ , some (small) variation with stellar parameters cannot be ruled out.

*Subject headings:* globular clusters: individual (M 68) — Hertzsprung-Russell diagram — open clusters: individual (M 67) — stars: atmospheres — stars: fundamental parameters (temperatures) — stars: evolution — Sun: abundances

## 1. Introduction

Nearly all published stellar models, including the large grids of evolutionary calculations by Girardi et al. (2000), Yi et al. (2001), Pietrinferni et al. (2004), and Vandenberg, Bergbusch, & Dowler

(2006), have described the atmospheric layers using either the  $T(\tau, T_{\text{eff}})$  relation from an empirical solar atmosphere (Krishna Swamy 1966; hereafter KS66 — see his equation 33), or that obtained for a gray atmosphere when the Eddington approximation is assumed.<sup>1</sup> As noted by, e.g., VandenBerg (1991) and Salaris, Cassisi, & Weiss (2002), just this difference alone can affect the predicted  $T_{\text{eff}}$  scale by up to  $\sim 100$  K. Consequently, models that treat the atmosphere differently must also adopt different values for the mixing-length parameter,  $\alpha_{\text{MLT}}$ , in order to satisfy the solar constraint. This, in turn, will have important ramifications for the predicted temperatures of giants, in particular, since the location of the red giant branch (RGB) on the H-R diagram is known to be a sensitive function of  $\alpha_{\text{MLT}}$  (see, e.g., VandenBerg 1983). In view of the critical role played by the atmosphere in calculations of stellar structure and evolution, it is obviously important to treat the outermost layers as accurately as possible.

The most straightforward way of avoiding, or at least minimizing, the systematic errors that must occur when a fixed  $T(\tau, T_{\text{eff}})$  relation is used to describe the temperature distribution in the surface layers is instead to attach modern model atmospheres onto interior structures. In this way, the differential effects of changes in the fundamental atmospheric parameters ( $T_{\text{eff}}$ , surface gravity, and chemical composition) are hopefully incorporated in the predicted  $T$ - $\tau$  structures. Preferably, atmospheres should be attached to interior models at large optical depths where the diffusion equation, which is the limiting form of the transfer equation that is solved by a stellar structure code, is valid. By comparing the radiative flux given by the diffusion equation with the exact values from model atmospheres, Morel et al. (1994) showed that the two determinations agree only at  $\tau \gtrsim 10$  in the case of solar-type stars, and at  $\tau \gtrsim 20$  in stars of very low gravity. However, the impact of matching atmosphere and interior models at smaller optical depths appears to be quite minor. Montalbán et al. (2001) reported that evolutionary tracks for  $0.8M_{\odot}$  stars having  $Z = 0.0002$  differed only slightly when model atmospheres were joined to interior models at  $\tau = 1, 10, \text{ or } 100$ . Much bigger effects on predicted temperatures were found if convection was treated differently in the atmosphere than in the interior, which suggests that it is very important to model the entire star as consistently as possible.

In fact, most studies to date of the consequences of using model atmospheres as boundary conditions have not had complete consistency between the atmosphere and interior models,

---

<sup>1</sup>In this investigation, the Greek letter  $\tau$  is used, without exception, to represent the Rosseland mean optical depth. In addition, the term “photosphere” is used here to refer to that layer in a star where the local temperature equals the effective temperature. (This definition is generally employed by those who construct stellar interior models.) Thus, it should be understood that, e.g., the “photospheric pressure” is the pressure at  $T = T_{\text{eff}}$ .

insofar as the adopted physics and/or chemical abundances are concerned. This includes the work by VandenBerg et al. (2000), who found that evolutionary tracks for metal-deficient  $0.8M_{\odot}$  stars were offset to warmer temperatures, by amounts that increased with decreasing  $[\text{Fe}/\text{H}]$ , when MARCS model atmospheres from the late 1990s were used to describe the surface layers instead of the KS66  $T(\tau, T_{\text{eff}})$  relationship. Salaris, Cassisi, & Weiss (2002) showed that giant branches utilizing Kurucz model atmospheres tended to be steeper than those obtained on the basis of gray or KS66  $T$ - $\tau$  structures, but it was also pointed out that the treatment of convection in the atmospheres that they employed was not the same as in their interior models. The same inconsistency was acknowledged to be a concern in the study of  $\alpha$ -element enhanced stellar models by Cassisi et al. (2004). Whether or not the noted inconsistencies have a large or small effect on the comparisons that were presented in those investigations is not known.

A follow-up study is clearly warranted — one in which the atmosphere and interior models assume exactly the same treatment of convection, the same abundances of helium and the most important heavy elements, and (as much as is practically possible) the same opacities and thermodynamics. In order to explore the consequences of fully consistent atmosphere-interior models for, in particular, the predicted temperatures of stars, the Victoria stellar structure code (see VandenBerg et al. 2006, and references therein) has been modified to use model atmospheres produced by the latest version of the MARCS code (e.g., see Gustafsson et al. 2003<sup>2</sup>) as boundary conditions. As shown in § 2, which is primarily concerned with numerical methods, the physical quantities predicted by these two codes are in excellent agreement when the same chemical abundances are assumed. § 3 presents several evolutionary sequences applicable to the Sun wherein the surface layers are treated in three different ways; namely, MARCS atmospheres, as well as the often-used gray and scaled-solar  $T(\tau, T_{\text{eff}})$  descriptions (e.g., KS66). This section also examines the impact on solar tracks of adopting either the new solar abundances derived by M. Asplund and collaborators from 3-D, non-LTE analyses of the solar spectrum (for a summary, see Asplund, Grevesse, & Sauval 2006) or the standard abundance distribution that was published by Grevesse & Sauval (1998) prior to the aforementioned work. In addition, the inferred temperatures of M 67 giants from  $V - K$  photometry suggest a preference for MARCS model atmospheres that have been corrected semiempirically so as to better represent the solar atmosphere. § 4 contains a similar analysis of the effects of variations in the treatment of the atmosphere for

---

<sup>2</sup>Many improvements have been to this computer program since 2003: they will be described in a forthcoming paper. Note, as well, that MARCS model atmospheres cooler than 4000 K are still in development at the present time; consequently, evolutionary models for stars with masses  $\lesssim 0.6M_{\odot}$  are not considered in this investigation. However, reference may be made to, e.g., Baraffe et al. (1997) and Brocato, Cassisi, & Castellani (1998) for some discussion of models for very low mass stars that take recent model atmospheres into account.

the tracks of metal-poor stars, and for isochrones appropriate to the globular cluster M 68, while concluding remarks are given in § 5.

## 2. Numerical Methods and Consistency Tests

### 2.1. Convection, Solar Metal Abundances, Opacities

Although the local mixing-length theory (MLT) of convection (Böhm-Vitense 1958) is employed by both the MARCS model atmosphere and the Victoria stellar evolution codes, a consistent treatment of convection would *not* be obtained if both computer programs adopted the same value of the free parameter,  $\alpha_{\text{MLT}}$ . This is for the reason that the most general form of the MLT (Henyey, Vardya, & Bodenheimer 1965) contains many other parameters, including (in particular)  $y$  and  $\nu$ , which describe the temperature distribution and the energy dissipation of a convective bubble, respectively. (Henyey et al. also define a quantity  $\beta$ , which is used to determine the turbulent pressure from the convective velocity, and they suggest using a correction to the diffusion equation denoted by  $f$ .) Whereas the MARCS code has generally adopted  $y = 0.076$  and  $\nu = 8$  over the years, the stellar models generated by the Victoria code have nearly always assumed  $y = \frac{1}{3}$  and  $\nu = 8$ . As shown by Pedersen, VandenBerg, & Irwin (1990), it is possible to compensate for a difference in  $y$  (or  $\nu$ , for that matter) by adjusting the value of  $\alpha_{\text{MLT}}$  appropriately. However, the generalized version of the MLT is included in the Victoria code, and hence  $y$  can simply be set to the default value used in the MARCS code (i.e., 0.076). Both codes will then have the same treatment of convection if they each assume identical values of  $\alpha_{\text{MLT}}$ .

The Sun is traditionally used to calibrate  $\alpha_{\text{MLT}}$  because it is the only star for which the fundamental parameters are sufficiently well determined. However, the value that is obtained for  $\alpha_{\text{MLT}}$  will depend on the adopted metal abundance, an initial helium content that is determined from the requirement that a  $1.0M_{\odot}$  model for the assumed metallicity reproduces the solar luminosity at the solar age, and the treatment of the atmosphere. Stellar evolution codes typically consider only the 19 metals listed in the first column of Table 1 because they, along with H and He, constitute the entire set of elements for which OPAL Rosseland mean opacities (Iglesias & Rogers 1996) may be computed for stellar interior conditions using the Livermore Laboratory website facility.<sup>3</sup>

In a concurrent study, VandenBerg et al. (2007) examined the fits of isochrones to the M 67 color-magnitude diagram, assuming the same chemical abundances adopted in

---

<sup>3</sup>See <http://www-phys.llnl.gov/Research/OPAL/>.

this study; i.e., the  $\log N$  abundances (on the scale where  $\log N_{\text{H}} = 12.0$ ) listed in the last two columns of Table 1. These give, in turn, the solar abundances published by Grevesse & Sauval (1998) and the distribution that is obtained when the revised abundances for several of the elements, as derived by M. Asplund and collaborators from analyses of the photospheric spectrum using 3-D, non-LTE model atmospheres, are taken into account. (Note that the entries for C and N in the third column are higher by 0.02 dex than the estimates published by Asplund, Grevesse, & Sauval 2006). The opacities computed by Vandenberg et al. are also used here — not only OPAL data for temperatures greater than  $\log T \sim 3.8$ , but also complementary opacities for lower temperatures, which include the contributions from molecules and grains. The low- $T$  opacities were calculated for the same heavy-element mixtures using the computer program described by Ferguson et al. (2005).

## 2.2. The Implementation of Atmospheric Boundary Conditions

Before discussing the calculation of Standard Solar Models, it is useful to summarize how the Lagrangian version of the Victoria evolutionary code operates (also see Vandenberg 1992). The usual stellar structure equations are solved by the Henyey method (Henyey, Forbes, & Gould 1964) only in the region of the star containing the innermost 99% of its mass. Two boundary conditions:

$$\log \mathcal{R} = a_1 \log P + a_2 \log T + a_3$$

and

$$\log \mathcal{L} = b_1 \log P + b_2 \log T + b_3$$

(where  $\mathcal{R}$  and  $\mathcal{L}$ , in units of  $10^{11}$  cm and  $10^{33}$  erg/s, are the adopted radius and luminosity variables, respectively) are added to the system of difference equations at  $\mathcal{M} = 0.99 \mathcal{M}_{\star}$ , while two additional boundary conditions are applied at, or near, the star’s center. To determine the coefficients  $a_i$  and  $b_i$ , Runge-Kutta integrations of 3 of the 4 stellar structure equations (assuming that the integrated luminosity is constant in the surface layers) are performed at three points on the H-R diagram that enclose the approximate  $L$  and  $T_{\text{eff}}$  of the model under consideration.

To begin these integrations it is necessary to have initial values for the temperature, radius, and pressure. If the starting point is taken to be the photosphere, then  $T_{\text{initial}} = T_{\text{eff}}$ ,  $\mathcal{R}_{\text{initial}}$  can be calculated from  $L = 4\pi R^2 \sigma T_{\text{eff}}^4$ , and  $P_{\text{initial}}$  may be determined either by (i) integrating the hydrostatic equation ( $\frac{dP}{d\tau} = \frac{g}{\kappa}$ ) from very small optical depths to the value of  $\tau$  where  $T = T_{\text{eff}}$ , on the assumption that the temperature distribution obeys the KS66 (or gray)  $T(\tau, T_{\text{eff}})$  relation, or (ii) interpolating in tables of photospheric pressures obtained from fully consistent model atmospheres that have been computed for a sufficiently wide

range in  $\log g$  and  $T_{\text{eff}}$ . If model atmospheres are attached at depth (e.g., at  $\tau = 100$ ), then the interpolations in the grids of model atmospheres must provide the initial values of  $T$ ,  $\mathcal{R}$ , and  $P$  at the chosen fitting point. (Because the flux has a  $1/r^2$  dependence, the values of the physical variables at depth will have some errors associated with them when the atmospheres are very thick, if derived from 1-D, flux-constant model atmospheres. However, as discussed in § 3.3, this is not a concern for the stellar models presented in this study.)

In practice, an additional equation must be defined at the end-point of the Runge-Kutta integrations so that the radius of the stellar model may be calculated once the Henyey scheme has converged: that equation is  $\log r/R = c_1 \log P + c_2 \log T + c_3$ . (As for the boundary conditions, three integrations down to  $0.99\mathcal{M}_*$  yield the values of  $\log r/R$ ,  $\log P$ , and  $\log T$  that are needed to define three equations involving the unknown quantities,  $c_1$ ,  $c_2$ , and  $c_3$ , which may be solved using standard methods.) As the model moves along its evolutionary track, the three points on the H-R diagram are adjusted, as necessary (using, e.g., the triangle strategy of Kippenhahn, Weigert, & Hofmeister 1967), so that the triangle they define always encloses the evolving model, and the “surface” boundary conditions are recomputed.

### 2.3. Standard Solar Models

The calculation of Standard Solar Models that made use of MARCS model atmospheres proceeded in the following way. For initial estimates of the values of  $\alpha_{\text{MLT}}$  and  $\log N_{\text{He}}$  that apply to the Sun, a small grid of model atmospheres (for effective temperatures ranging from 5500 K to 6250 K, in steps of 250 K, and, at each  $T_{\text{eff}}$ ,  $\log g$  values from 4.0 to 4.9, in steps of 0.3 dex) was calculated. An evolutionary track for a  $1.0\mathcal{M}_\odot$  star was then computed from the zero-age main sequence (ZAMS) to an age of 4.6 Gyr using the MARCS atmospheres as boundary conditions (via the methods described above). The solar-age model so obtained would generally fail to reproduce the properties of the Sun (specifically, its luminosity and  $T_{\text{eff}}$ ) satisfactorily. As a result, the trial values of  $\alpha_{\text{MLT}}$  and  $\log N_{\text{He}}$  were revised, the small grid of model atmospheres was recomputed to be consistent with updated values of these parameters, and a new solar track was calculated. After a few iterations, a solar model was obtained that reproduced the observed  $\log L$  and  $\log T_{\text{eff}}$  values to within 0.0002 dex.

This procedure was repeated for each of the two heavy-element mixtures given in Table 1, resulting in the values of  $\alpha_{\text{MLT}}$ ,  $\log N_{\text{He}}$ ,  $X$ ,  $Y$ , and  $Z$  contained in Table 2. (The model atmospheres and low-T opacities consider many more elements than those listed in Table 1, but they do not affect the overall mass-fraction abundances appreciably because their abundances are low. Their effects on the blanketing and opacity are, however, taken into account.)

## 2.4. Comparison of Results from the MARCS and Victoria Codes

To check the consistency of the MARCS and Victoria codes, both computer programs were used to calculate the structure of the sub-photospheric layers of the Sun. In Figure 1, the solid curves indicate the predicted  $T$ ,  $P$ , opacity,  $\dots$  profiles between the photosphere and that layer where  $\tau = 100$  as predicted by the MARCS atmosphere code for a star having  $\log g = 4.44$ ,  $T_{\text{eff}} = 5777$  K, the Asplund mix of heavy elements, and the values of  $\alpha_{\text{MLT}}$  and  $\log N_{\text{He}}$  given in Table 2. The dashed curves, on the other hand, represent the results of Runge-Kutta integrations by the Victoria evolutionary code inward from the solar photosphere for the same abundances and parameter values, and assuming that the initial values of the dependent variables are the predicted pressure at  $T = T_{\text{eff}}$  from the MARCS model, the observed  $T_{\text{eff}}$ , and the observed radius of the Sun. The agreement between the two is clearly excellent, which demonstrates that the effects of differences in the physics implemented in the two codes are very minor. (A similar comparison was carried out for a model on the lower RGB having  $T_{\text{eff}} = 4726$  K and  $\log g = 3.45$ , and the results were qualitatively almost identical.)

To be sure, some variations are expected because, in particular, the diffusion equation approximation to the transfer equation is used in the Victoria code, while the MARCS code solves the monochromatic form of the transfer equation for  $\sim 10^5$  wavelength points. In fact, the small discrepancies in the temperature profiles in Fig. 1, are consistent with this difference. Using the diffusion approximation together with Rosseland mean opacities *should* lead to a shallower temperature gradient at  $\tau \lesssim 1$  than that predicted by model atmospheres. As discussed by, e.g., Mihalas (1970), a better approximation to the true gradient would be obtained if the larger Planck means were used in the outer layers. In any case, the level of consistency between the MARCS and Victoria codes is clearly very satisfactory, and we can be confident that the atmosphere and interior structures are about as well matched as it is possible to make them.

## 2.5. On the Mass Dependence of Model Atmospheres

We conclude this section with a few comments on the question of whether a model atmosphere has any direct dependence on the assumed mass in addition to its dependence on surface gravity. For a plane-parallel model, the mass is not defined and the radius, in principle, is infinite. Plane-parallel stratification is a reasonable approximation when the atmospheric geometrical depth is a very small fraction of the star’s radius, as in dwarfs and subgiants. However, sphericity effects do introduce a mass dependence in very extended models. To illustrate this, spherical model atmospheres have been computed for  $T_{\text{eff}} = 4000$

K,  $\log g = 0.0$ ,  $Z = 0.05$ , and masses of  $0.5$  and  $5.0\mathcal{M}_\odot$  (which have total radii of  $117$  and  $371\mathcal{R}_\odot$ , respectively). The predicted  $T$ - $\tau$ , depth- $\tau$ , and  $T$ -depth structures for these two cases are shown in Figure 2. Because the atmosphere from  $\tau \sim 10^{-4}$  to  $\tau \sim 1$  is a much larger fraction of the total radius in the  $0.5\mathcal{M}_\odot$  star ( $\approx 20\%$ ) than in the  $5.0\mathcal{M}_\odot$  star ( $\approx 5\%$ ), the sphericity effects on the radiation field are considerably larger in the lower mass star. These cause reduced temperatures in the outermost layers and a steeper temperature gradient over most of the atmosphere, as evident in Fig. 2b. However, even in this fairly extreme example, the structures of the inner atmospheres (from the photosphere to  $\tau = 100$ , which is the main region of interest in this investigation) do not differ by very much. (For additional discussion concerning the effects of varying atmospheric extension, see Heiter & Eriksson 2006.)

### 3. Models for $[\text{Fe}/\text{H}] = 0.0$ Stars

Most of the following analysis of the impact of different treatments of the atmospheric layers on the structure and evolution of solar abundance stellar models assumes the Asplund mix of heavy elements (Table 1) and the corresponding  $X$ ,  $Y$ , and  $Z$  values given in Table 2. Models for the Grevesse & Sauval (1998; hereafter GS98) metals mixture are considered (in a separate subsection) mainly to illustrate the dependence of evolutionary tracks with consistent model atmospheres on the distribution of the elemental abundances when the atmospheric layers are treated similarly (i.e., by fully consistent MARCS models). Note that all evolutionary calculations presented in this paper assume that  $\alpha_{\text{MLT}}$  is independent of mass, metallicity, and evolutionary state, given that compelling evidence in support of any such dependence has not yet been found (see the summary of work to date on this issue by Ferraro et al. 2006<sup>4</sup>).

#### 3.1. Solar Abundance Models, Assuming $Z_\odot = 0.01247$ (Asplund)

Having determined the helium abundance and the value of  $\alpha_{\text{MLT}}$  needed to fit the Sun (see § 2.3 and Table 2), it is a straightforward exercise to produce evolutionary tracks for

---

<sup>4</sup>These authors suggest that there *may* be a difference in the value of  $\alpha_{\text{MLT}}$  that must be assumed in stellar models to reproduce the temperatures of globular cluster giants, as derived from  $V - K$  photometry, and that required by a Standard Solar Model, *if* the new Asplund metal abundances for the Sun are assumed. Such inferences are highly speculative because they are subject to the large uncertainties that persist in the cluster  $[\text{Fe}/\text{H}]$  scale and the treatment of the atmospheric layers in stellar models, among other things. Ample support for this assertion is provided in the present study.

solar parameters that extend to the lower RGB. To achieve this, a much larger grid of model atmospheres (for  $4000 \leq T_{\text{eff}} \leq 8000$  K and  $3.0 \leq \log g \leq 5.0$ , in steps of 250 K and 0.5 dex, respectively) was computed, assuming the Asplund abundances and the calibrated values of  $\log N_{\text{He}}$  and  $\alpha_{\text{MLT}}$ . The tracks for a  $1.0M_{\odot}$  model that were obtained when these atmospheres were fitted to interior structures at the photosphere, on the one hand, and at  $\tau = 100$ , on the other, are shown in Figure 3 as solid and dashed curves. The two evolutionary sequences are nearly identical, which implies that, at least for this case, the derived  $T_{\text{eff}}$  scale is essentially independent of the fitting point.

Also plotted in Fig. 3 are evolutionary tracks for the same mass,  $Y$ , and  $Z$  in which either the KS66  $T(\tau, T_{\text{eff}})$  relation (the dotted curve) or that for a gray atmosphere (dot-dashed curve) is used to describe the atmospheric layers exterior to the photosphere. In both of these cases, the mixing-length parameter was chosen so that the solar constraint was satisfied: hence all of the tracks are coincident at the location of the solar symbol. Interestingly, the track using gray atmospheres lies very close to those employing MARCS model atmospheres, while the giant branch of the track using KS66 atmospheres is hotter than the rest by  $\sim 100$  K. In fact, these results are a consequence of the differences in the assumed values of  $\alpha_{\text{MLT}}$ .

This can be readily substantiated with the aid of Figure 4, which compares the evolutionary sequences that are obtained for the three different treatments of the atmospheric layers considered in Fig. 3 when the same value of the mixing-length parameter is assumed. Whereas, to first order, changes in the treatment of the atmosphere shift an entire track by a roughly constant amount in  $T_{\text{eff}}$ , varying  $\alpha_{\text{MLT}}$  has a 2–3 times larger impact on the temperatures of giants than on the temperatures of main-sequence stars (see, e.g., Fig. 5 by VandenBerg 1991). In Fig. 4, the dot-dashed curve is closer to the solid curve in the vicinity of the main sequence than along the RGB, while the opposite is true in the case of the dotted curve. It is, therefore, to be expected that the dot-dashed curve will end up being just slightly cooler, and the dotted curve considerably hotter, than the solid curve, once  $\alpha_{\text{MLT}}$  has been suitably normalized using the Sun (as in Fig. 3).

However, Fig. 4 is itself problematic. Because the KS66  $T(\tau, T_{\text{eff}})$  relation is based on an empirical solar atmosphere, one would expect that the solid and dotted curves should be nearly coincident, especially at luminosities and temperatures close to that of the Sun. That they are not in particularly good agreement is presumably a consequence of the fact that modern 1-D, plane-parallel model atmospheres employing the local mixing-length theory of convection are unable to reproduce the actual  $T$ – $\tau$  structure of the Sun adequately. For instance, Blackwell, Lynas-Gray, & Smith (1995) have shown that the limb darkening of a theoretical flux-constant solar model does not fit the observations (as compared with the scaled solar

model by Holweger & Müller 1974; hereafter HM74) very well (though, interestingly, 3-D models of the solar atmosphere are more successful; see Asplund, Nordlund, & Trampedach 1999).

To ensure that there is no significant dependence of the results on the particular empirical solar atmosphere that is assumed, the dotted curve was recomputed using the HM74 model as represented by Vandenberg & Poll (1989). This solar atmosphere is preferable to that given by KS66 because the former, but not the latter, is known to reproduce the solar flux and limb darkening quite well. [The KS66  $T(\tau, T_{\text{eff}})$  relation was derived solely from a consideration of spectral line profiles.] The resultant track (not shown here) agreed with that based on KS66 atmospheres all the way from the ZAMS to the highest luminosity plotted in Fig. 3 to within  $\approx 0.0008$  in  $\log T_{\text{eff}}$  (or  $\approx 10$  K). Of course, to compensate for this small offset in temperature, some adjustment in the assumed value of  $\alpha_{\text{MLT}}$  (to 1.96) would be needed to obtain a Standard Solar Model with an HM74 atmosphere. (The required small decrease in the value of the mixing-length parameter results in the giant-branch segment of the solar track for the HM74 case being  $\approx 20$  K cooler at  $M_{\text{bol}} = 2.2$  than the dotted curve.)

Differences in the predicted pressures at  $T = T_{\text{eff}}$  are the main cause of the separations (in the horizontal direction) between the three tracks presented in Fig. 4. As shown in Figure 5, which plots the structures of the sub-photospheric layers (down to  $\tau \sim 100$ ) in Standard Solar Models having MARCS, gray, or KS66 atmospheres, the photospheric pressures and the variations of  $T$  and  $P$  with depth differ markedly in the three cases considered. (All models must replicate the observed temperature of the Sun at the photosphere, defined here to coincide with zero depth.) The best estimate of the pressure at  $T = T_{\text{eff}}$  is arguably that indicated by the open circle since it has been derived from an empirical solar atmosphere. [Furthermore, because the calibration of the mixing-length parameter should be based on the most realistic solar model that can be computed, the preferred estimate of  $\alpha_{\text{MLT}}$  ( $\approx 2.0$ , assuming the Asplund estimate of  $Z_{\odot}$ ) is obtained when a reliable empirical solar atmosphere is used in the computation of a Standard Solar Model instead of, for instance, a gray or a MARCS atmosphere.] Unfortunately, it is not known how the physics in MARCS atmospheres should be modified so that they predict suitably reduced pressures at the photosphere. Regardless of how it is achieved, a significant reduction in the photospheric pressure that is predicted by the MARCS solar atmosphere is needed to achieve consistency with models for the Sun having KS66 (or HM74) atmospheres.

While there is no reason to expect that the same adjustment to the photospheric pressure should be made at all effective temperatures and gravities, such an assumption has the intriguing consequence that the resultant evolutionary sequences are a close match to those obtained when the KS66  $T(\tau, T_{\text{eff}})$  relation is used to derive the boundary pressure. This is

illustrated in Figure 6, which compares a solar track that assumes KS66 atmospheres and  $\alpha_{\text{MLT}} = 2.0$  (the dotted curve) with three different tracks that employ MARCS atmospheres. The solid and dashed curves assume that  $\alpha_{\text{MLT}} = 1.80$  and  $2.00$ , respectively, while the dot-dashed curve is otherwise identical to the dashed curve except that the predicted pressures at  $T = T_{\text{eff}}$  are reduced by  $\delta \log P = 0.1375$  (i.e., the difference between the open and filled circles in Fig. 5). It is quite remarkable that the last of these cases reproduces the KS66 track so well, despite the variations in the  $T$ – $\tau$  structures that must exist as a function of  $T_{\text{eff}}$  and gravity. Such variations apparently do not have important consequences for the photospheric pressure in a systematic sense.

It was, in fact, not necessary to have completely consistent atmosphere-interior models insofar as the assumed value of the mixing-length parameter is concerned. As shown in Figure 7, which plots the  $T$ –depth and  $P$ –depth profiles predicted by MARCS atmospheres for the sub-photospheric layers in models for solar parameters and  $\alpha_{\text{MLT}} = 1.50, 1.80,$  and  $1.92$ , the predicted photospheric pressure is independent of  $\alpha_{\text{MLT}}$ . Moreover, since nearly the same evolutionary tracks are obtained when MARCS atmospheres are attached to interior models at the photosphere or at  $\tau = 100$  (as shown in Fig. 3), there is little to be gained by making this attachment at depth (provided that the atmosphere and interior codes incorporate very similar physics: some counter-examples are discussed below). The key ingredient to be obtained from these particular model atmospheres is the photospheric pressure.

If the loci in Fig. 5 for the various Standard Solar Models are extended to  $0.99\mathcal{M}_{\odot}$  by integrating the stellar structure equations, and the resultant  $\log T$  and  $\log P$  values are plotted as a function of  $\log r$  (instead of depth), one obtains Figure 8. The inner atmosphere of the Sun (i.e., between the photosphere and the point where  $\tau = 100$ ) is clearly a very thin layer. Indeed, because a depth of  $\sim 16 \times 10^6$  cm below the photosphere (see Fig. 5) represents only  $\sim 0.02\%$  of the radius of the Sun, the relatively large differences between the various loci plotted in Fig. 5 are not discernible in Fig. 8. Importantly, all of the integrations yield essentially the same values of temperature, pressure, and radius at  $0.99\mathcal{M}_{\odot}$  (and, in fact, nearly identical radial variations of  $T$  and  $P$ ).

To illustrate the dependence of the integrations down to  $0.99\mathcal{M}_{\odot}$  on the adopted value of  $\alpha_{\text{MLT}}$ , the case represented by the filled circle, and assuming the photospheric pressure from the MARCS model atmosphere, was repeated using  $\alpha_{\text{MLT}} = 1.71$  instead of  $1.80$  (the value required by a Standard Solar Model). This resulted in the dotted curves, which are actually quite close to the others that have been plotted, and the values of  $\log T$ ,  $\log P$ , and  $\log r$  at  $0.99\mathcal{M}_{\odot}$  indicated in Fig. 8 by the filled squares. Because the latter are significantly displaced from the filled circles, the resultant boundary conditions are also quite different, resulting in a solar model that is  $\sim 40$  K cooler than the Sun. (This offset is in the expected

direction when the assumed value of  $\alpha_{\text{MLT}}$  is less than that needed to satisfy the solar constraint; see Fig. 4).

### 3.1.1. *The Effects of Macroturbulence in Model Atmospheres*

The MARCS model atmospheres considered thus far did not take into account one component to the pressure that is normally included; namely, the pressure arising from macroturbulence, which is due to relatively large scale motions in the stellar atmosphere. (This was disregarded to improve the consistency with the interior models produced by the Victoria code, since the latter does not treat this additional physics.) In the MARCS code, the turbulent pressure is calculated from  $P_{\text{turb}} = 0.5 \rho v^2$ , where  $v$  is the characteristic velocity and  $\rho$  is the density (for some discussion of this equation, see Henyey et al. 1965). The model atmospheres computed for this study assume that  $v = (6.5 - \log g)$  km/s. (The inclusion of  $P_{\text{turb}}$  with such depth-independent values of  $v$  corresponds closely to a shift in the surface gravities of models with no macroturbulence, cf. Gustafsson et al. 1975: matters are more complicated if  $v$  is assumed to vary with depth.)

However, it seems to be the case that taking a turbulent component to the pressure into account has no more than a small effect on the predicted  $T_{\text{eff}}$  scale. Figure 9 compares the structures of the sub-photospheric layers given by MARCS model atmospheres for solar parameters ( $\log g = 4.44$ ,  $T_{\text{eff}} = 5777$  K, and Asplund abundances), computed with and without the inclusion of turbulent pressure but assuming the same value of the mixing-length parameter ( $\alpha_{\text{MLT}} = 1.77$ , which is needed to produce a Standard Solar Model when the turbulent pressure is included in the atmosphere). The differences in the various quantities are appreciable, though not large enough to have a big impact on stellar evolutionary models. As shown in Figure 10, the tracks that are obtained when turbulent MARCS atmospheres are used as boundary conditions differ only slightly from those employing non-turbulent atmospheres. (At  $M_{\text{bol}} = 2.3$ , the dotted and dot-dashed curves differ in temperature by  $\approx 30$  K.) This similarity is due, in part, to the fact that the former calculations assume a somewhat smaller value of  $\alpha_{\text{MLT}}$  than the latter (in order to reproduce the properties of the Sun at the solar age), which thereby compensates for some of the effects due to the difference in physics.

There is an additional parameter (besides those associated with the mixing-length treatment of convection) that can be varied in the model atmosphere code; namely, the microturbulence, which affects the spectral line blanketing. However, variations in this quantity have only a very minor effect on the predicted temperatures of stellar models. If, for instance, the assumed microturbulent velocity is changed from 1 km/s to 2 km/s, the predicted photo-

spheric pressure of the Sun (or of a model on the lower RGB) decreases by  $\delta \log P = 0.007$ – $0.008$ . This change in the boundary pressure results in stellar models that have lower values of  $T_{\text{eff}}$  by only a few Kelvin.

### 3.2. Solar Abundance Models, Assuming $Z_{\odot} = 0.0165$ (GS98)

If the calculation of a solar evolutionary track is repeated assuming the GS98 heavy-element mixture and  $Y = 0.26764$  (see Table 2), which implies  $Z_{\odot} = 0.01651$ , together with  $\alpha_{\text{MLT}} = 1.84$  and boundary conditions based on fully consistent MARCS model atmospheres, the result is the dashed curve in Figure 11. This may be compared with the solid curve, which assumes the Asplund abundances for several of the elements heavier than helium (see Table 1) and the adopted values of the relevant parameters specified in Table 2. (This track is identical to those plotted as solid curves in Figs. 3, 4, and 10.) The third track that appears in Fig. 11 (the dotted curve) has been taken from the extensive grids of evolutionary models published by VandenBerg et al. (2006). In these calculations, the solar parameters were taken to be  $Y_{\odot} = 0.2768$ ,  $Z_{\odot} = 0.0188$  (assuming the mix of metals given by Grevesse & Noels 1993), and  $\alpha_{\text{MLT}} = 1.90$ . Moreover, the pressure at  $T = T_{\text{eff}}$  was determined by integrating the hydrostatic equation in tandem with the KS66  $T(\tau, T_{\text{eff}})$  description of the outer atmospheric layers.

As regards the three tracks in Fig. 11: the relative locations of the subgiant and giant branches are the expected consequences of the differences in the CNO abundances (see Rood & Crocker 1985), which are mainly responsible for the differences in  $Z$ , and in the adopted values of  $\alpha_{\text{MLT}}$ , respectively. Except for the RGB, the tracks are sufficiently similar that it is not possible to discriminate between them empirically. Indeed, the main conclusion to be drawn from this plot is that the predicted temperatures of solar abundance giants depend sensitively on the adopted value of  $Z_{\odot}$  (and the detailed heavy-element mixture), which is currently a subject of considerable controversy (see, e.g., Asplund et al. 2005, VandenBerg et al. 2007).

Whether or not the same value of the mixing-length parameter is appropriate for solar abundance giants as for the Sun must therefore depend on the value of  $Z_{\odot}$ . VandenBerg & Clem (2003) found that the effective temperatures of M 67 giants, as determined using empirical  $(V - K)$ – $T_{\text{eff}}$  relations, agreed very well with those predicted by a 4.0 Gyr,  $Z = 0.0173$  isochrone that assumed KS66 atmospheric structures. (In that study, the adopted value of  $Z_{\odot}$  was 0.0188 and M 67 was assumed to have  $[\text{Fe}/\text{H}] = -0.04$ , in which case, the corresponding value of  $Z$  is 0.0173.) Because the prediction of stellar temperatures is so central to this investigation, it is worthwhile to revisit this constraint.

### 3.3. The Temperatures of M 67 Giants and Their Implications for the Predicted $T_{\text{eff}}$ Scale

If we adopt  $E(B - V) = 0.038$  and  $(m - M)_V = 9.70$ , together with  $E(V - K) = 2.78 E(B - V)$ ,  $A_V = 3.12 E(B - V)$  and  $A_K = 0.34 E(B - V)$  (Bessell & Brett 1988), it is a trivial task to obtain  $M_V$  and  $(V - K)_0$  values for the giants in M 67 for which  $VK$  photometry has been reported by Houdashelt, Frogel, & Cohen (1992). (The assumed reddening and distance modulus are believed to be current best estimates; see the discussion of cluster parameters provided by Vandenberg et al. 2007.) The temperatures then follow from the empirical relations between  $(V - K)$  and  $T_{\text{eff}}$  given by Bessell, Castelli, & Plez (1998) and van Belle et al. (1999), which are based on the latest determinations of stellar radii from lunar occultations and Michelson interferometry. The resultant  $(\log T_{\text{eff}}, M_V)$ -diagram is shown in the left-hand panel of Figure 12. Note that, at the  $M_V$  value of each star, the temperatures derived from the Bessell et al. and van Belle et al. color transformations are plotted as open and closed circles, respectively.

The dotted curve is the RGB segment of the same 4.0 Gyr,  $Z = 0.0173$  isochrone that provided a very good fit to the M 67 CMD in the Vandenberg & Clem (2003) study. It matches the distribution of cluster giants quite well, particularly if compared with the luminosity and temperature data indicated by the filled circles. (The small group of stars at  $\log T_{\text{eff}} \approx 3.675$  and  $M_V \approx 0.9$  plays no role in this comparison because they are almost certainly horizontal-branch stars.) However, this constraint is not nearly as stringent as one would like. Although the temperatures of many of the stars used in current calibrations of  $(V - K)$  versus  $T_{\text{eff}}$  have been determined to better than  $\sim 1.3\%$ , the standard deviation of the measured values of  $T_{\text{eff}}$  at a given  $V - K$  color is typically 7% (van Belle et al. 1999). Such large uncertainties clearly permit considerable leeway in the models.

The solid and dashed curves represent, in turn, the giant-branch extensions of 4.2 Gyr,  $Z = 0.01247$  (Asplund) and 3.9 Gyr,  $Z = 0.01651$  (GS98) isochrones that were compared with the Montgomery, Marschall, & Janes (1993) CMD of M 67 by Vandenberg et al. (2007). [The models used in that study are completely consistent with those presented here; indeed, the tracks for  $1.0M_{\odot}$  are identical. Interestingly, only the high- $Z$  isochrone predicts a gap where one is observed in M 67 — which is potentially a problem for the Asplund estimate of  $Z_{\odot}$ , since this open cluster is known to have very close to solar metal abundances (e.g., see the results of high-resolution spectroscopy reported by Hobbs & Thorburn 1991; Tautvaišienė et al. 2000; Randich et al. 2006). However, as noted by Vandenberg et al., isochrones for the Asplund metallicity *may* provide a good match to the M 67 CMD in the vicinity of the turnoff if diffusive processes are treated: further work is needed to investigate this possibility. Aside from the turnoff, the 4.2 and 3.9 Gyr isochrones for the Asplund and

GS98 metallicities provide equally satisfactory fits to the cluster main sequence and subgiant branch; see the VandenBerg et al. paper.]

There is little doubt that the predicted temperatures along these loci are too cool (which could be taken as evidence that  $\alpha_{\text{MLT}}$  is larger in solar abundance giants than in main-sequence dwarfs;<sup>5</sup> however, see below). The extension of the evolutionary sequences and isochrones to  $M_V \sim -1$  required the calculation of complementary grids of model atmospheres for  $4000 \leq T_{\text{eff}} \leq 5500$  K and  $0.0 \leq \log g \leq 2.5$  in steps of 250 K and 0.5 dex, respectively. [Note that, as shown in the right-hand panel of Fig. 12, the discrepancies found by VandenBerg et al. 2007 between the isochrones represented by the solid and dashed curves and the faintest cluster giants on the  $[(B - V)_0, M_V]$ -plane persist to higher luminosities. Moreover, the close similarity of the comparisons between theory and observations presented in both panels of this figure indicates that the adopted  $(B - V)$ - $T_{\text{eff}}$  relations (from VandenBerg & Clem 2003) are consistent with the empirical  $(V - K)$ - $T_{\text{eff}}$  relationships.]

A set of spherical model atmospheres were also computed (for temperatures from 4000 K to 4750 K and  $1.0 \leq \log g \leq 2.5$ ) to enable us to determine whether their use as boundary conditions resulted in tracks for upper-RGB stars that differed in any significant way from those employing plane-parallel atmospheres. The differences between the models that incorporated the two different types of model atmospheres were found to be barely discernible, which demonstrates that sphericity effects are very small and of little consequence for the evolutionary calculations presented in this investigation. The dot-dashed curve in Fig. 12 is also based on MARCS model atmospheres, and it is able to reproduce the properties of M 67 giants (and the Sun) just as well as the dotted curve (on the assumption of a constant value of  $\alpha_{\text{MLT}}$ ). The SDC variant of MARCS models, upon which the dot-dashed RGB is based, is introduced in the next section.

### 3.4. Using MARCS SDC Atmospheres as Boundary Conditions

Since, as already noted, the MARCS solar atmosphere does not reproduce the observed flux and limb darkening of the Sun as well as the HM74 solar atmosphere, it could be argued that HM74 models, when scaled to the appropriate  $T_{\text{eff}}$ , provide the best representations

---

<sup>5</sup>Indeed, the 2-D hydrodynamical simulations of Ludwig, Freytag, & Steffen (1999) suggest that the proper mixing-length to adopt for giants and subgiants is  $\sim 0.1$  greater than that for solar-type stars. Following VandenBerg (1991), we estimate that such a change would bring the model RGB that employs MARCS atmospheres about half-way to the observed sequence in Fig. 12. More realistic 3-D models, already available today (Collet et al. 2007), should be used to further illuminate this possibility.

of solar-type stars (provided that the pressure is obtained by integrating the hydrostatic equation at the relevant surface gravity). However, MARCS models have the important advantage that changes in the opacity distributions across the spectrum, and with depth, on the radiative energy transfer are handled properly by the MARCS code, at least within the adopted LTE and 1-D assumptions. These opacity variations occur systematically with  $T_{\text{eff}}$ , surface gravity, and chemical composition; consequently, these differential changes should be taken into account if models with different fundamental parameters are related — as they are along our evolutionary tracks.

Thus, rather than adopting theoretical MARCS models directly, it may be preferable to use them in a strictly differential sense to correct the HM74 atmospheres for the effects of changes in the basic stellar parameters. Such “scaled solar, differentially corrected” (SDC) models would have temperature structures given by

$$T(\tau) = \left( \frac{T_{\text{eff}}}{T_{\text{eff}, \odot}} \right) T_{\text{HM74}}(\tau) + T_{\text{MARCS}}(\tau) - \left( \frac{T_{\text{eff}}}{T_{\text{eff}, \odot}} \right) T_{\text{MARCS}, \odot}(\tau) .$$

According to this equation, the HM74 solar atmosphere is first scaled to the correct effective temperature, and then a correction is applied given by the difference between the MARCS model at the relevant parameters and the corresponding scaled solar MARCS model. This equation is obviously equivalent to

$$T(\tau) = T_{\text{MARCS}}(\tau) + \left( \frac{T_{\text{eff}}}{T_{\text{eff}, \odot}} \right) [T_{\text{HM74}}(\tau) - T_{\text{MARCS}, \odot}(\tau)] ,$$

i.e., the adopted  $T(\tau, T_{\text{eff}})$  relation is obtained by correcting the relevant MARCS model by the *scaled* difference between the HM74 and MARCS solar atmospheres. All scaling is done with respect to the Rosseland mean optical depth: with the resultant  $T$ - $\tau$  structure so obtained, the equation of hydrostatic equilibrium is then integrated on the assumption of the relevant chemical composition and surface gravity to obtain the pressure as a function of depth in the atmosphere. Note that, for a model having solar parameters, the above equation reduces to  $T(\tau) = T_{\text{HM74}}(\tau)$ . (As already mentioned, it is preferable to use the HM74 atmosphere in this exercise, instead of that by KS66, because it has been much more thoroughly studied and found to provide good consistency with the observed flux, limb darkening, and spectral line profiles of the Sun.)

Because the HM74 solar atmosphere is not defined at optical depths greater than  $\tau = 10$ , where the uncertainties will already be large because so little of the observed light originates at such depths, we have opted to fit the MARCS SDC atmospheres to the interior models at  $\tau = 5$ . With just this change to the treatment of the atmospheric layers and the assumption of  $\alpha_{\text{MLT}} = 2.01$ , which is required to satisfy the solar constraint in this case, evolutionary

tracks that are otherwise identical to those plotted as solid curves in Fig. 13 were computed, along with an isochrone for 4.2 Gyr. Taken at face value, the giant-branch segment of this isochrone (the dot-dashed curve in Fig. 12) does the best job of all the cases that have been plotted in reproducing the observed RGB of M 67 (though the uncertainties in the data are too large to differentiate between the dotted and dot-dashed curves).

On the  $[(B - V)_0, M_V]$ -plane (see the right-hand panel of Fig. 12), the lower RGB segment of the dot-dashed isochrone is approximately mid-way between the dashed curve and the observed giant branch. (There is no obvious discrepancy in the left-hand panel, though only two stars fainter than  $M_V \sim 2$  have measured temperatures.) However, a difference  $\approx 0.03$ – $0.05$  mag in  $B - V$  at  $2 \lesssim M_V \lesssim 3.5$ , is within the uncertainties of current color– $T_{\text{eff}}$  relations. For instance, the transformations reported by Houdashelt, Bell, & Sweigart (2000) yield a value of  $B - V = 1.023$  for a star having  $[\text{Fe}/\text{H}] = 0.0$ ,  $T_{\text{eff}} = 4750$  K, and  $\log g = 3.0$  (which is appropriate for a lower RGB star in M 67), while  $B - V = 1.050$  is obtained from the  $(B - V)$ – $T_{\text{eff}}$  relations reported by Castelli (1999), on the assumption of the same stellar parameters. [For the reasons discussed by Vandenberg & Clem (2003), the Castelli transformations were considered to be more realistic, but that was a judgment call and not necessarily the right one (particularly if the Asplund value of  $Z_{\odot}$  is correct). At the same time, it should be appreciated that model-atmosphere-based synthetic colors generally do not agree well with those given by empirical color– $T_{\text{eff}}$  relations (e.g., Sekiguchi & Fukugita 2000), especially for cool stars. Consequently, it is not possible to obtain anywhere near as satisfactory a fit of isochrones to the entire CMD of M 67 as that presented by Vandenberg et al. (2006) using, for instance, either the Houdashelt et al. or the Castelli transformations. This is the reason why Vandenberg & Clem relied on empirical color– $T_{\text{eff}}$  relationships whenever it was possible to do so.] In any case, if the MARCS SDC atmospheres are assumed to be realistic boundary conditions, one may conclude that, at least for solar abundance stars,  $\alpha_{\text{MLT}}$  does not vary significantly (if at all) with changes in  $T_{\text{eff}}$  between 4000 K and 7000 K or in  $\log g$  values from 0.0 to 5.0.

Given that the effect of using SDC atmospheres for the Asplund metallicity as boundary conditions for stellar models is to move the predicted RGB from the location of the solid curve to that of the dot-dashed curve (see Fig. 12), one might anticipate that the use of SDC atmospheres for the GS98 abundances would imply a giant branch that is somewhat too hot/blue. This assumes that the separation, in the horizontal direction, between the latter and the dashed curve would be comparable to that between the dot-dashed and solid curves. We have not examined this possibility, mainly because the difference in  $T_{\text{eff}}$  between the dashed and solid curves is comparable to the uncertainty in the empirically derived temperatures (at least  $\pm 50$ – $100$  K). Thus, even if the predicted RGB for the GS98 case turned out to be  $\sim 75$  K hotter than the dot-dashed curve, it would still be within the

$1\sigma$  uncertainty of the measured temperatures of M 67 giants, and it would be incorrect to conclude, for instance, that models for giants must assume a smaller value of  $\alpha_{\text{MLT}}$  than those for dwarf stars. The observational and theoretical uncertainties are such that a small variation in  $\alpha_{\text{MLT}}$  with evolutionary state cannot be ruled out.

#### 4. Models for $[\text{Fe}/\text{H}] = -2.0$ Stars

To investigate the impact of using different treatments of the atmosphere on the predicted  $T_{\text{eff}}$  scale at low  $Z$ , evolutionary tracks have been computed for  $[\text{Fe}/\text{H}] = -2.0$ , on the assumption of the mix of heavy elements listed in Table 3. To obtain this particular mixture, the Asplund  $\log N$  abundances for the Sun (Table 2) were reduced by 2.0 dex and then adjusted appropriately so that the resultant  $[\text{m}/\text{H}]$  values (see the fourth column in Table 3) were close to the measured values in  $[\text{Fe}/\text{H}] \approx -2$  stars (see Cayrel et al. 2004). Note that most of the  $\alpha$  elements are enhanced by 0.3 dex (oxygen by 0.5 dex), while a few elements (Na, Cr, and Mn) are underabundant relative to a scaled-solar mixture. As far as helium is concerned,  $\log N_{\text{He}} = 10.92$  was assumed, so that the resultant mass-fraction abundances came out to be  $X = 0.75149$ ,  $Y = 0.248233$  (in agreement with the value implied by the concordance between WMAP and Big-Bang nucleosynthesis; see Coc et al. 2004), and  $Z = 2.8 \times 10^{-4}$ . Opacities and a set of MARCS model atmospheres for  $4000 \leq T_{\text{eff}} \leq 8000$  K and  $0.0 \leq \log g \leq 5.0$  were computed for these chemical abundances. Moreover,  $\alpha_{\text{MLT}} = 1.80$  was adopted, in both the atmosphere and interior models, in order to be consistent with the requirements of a Standard Solar Model. (Stellar models employing metal-poor MARCS SDC atmospheres are discussed below.)

It is well known (e.g., see Gustafsson et al. 1975; Irwin 1985) that convection extends to shallower (i.e., smaller) optical depths in a metal-poor atmosphere than in a metal-rich atmosphere having a similar  $T_{\text{eff}}$  and gravity. This raises the concern that models for metal-deficient stars may be much more dependent on where the atmospheres are attached to the interior structures (i.e., at the photosphere or at some deeper layer) than those for solar abundances. Indeed, Runge-Kutta integrations of the stellar structure equations, beginning at the photosphere, are not able to reproduce the predictions of metal-deficient model atmospheres for the deeper layers particularly well. This is shown in Figure 13, which compares the variations of several quantities in the sub-photospheric layers, as predicted by MARCS atmospheres for a star having  $T_{\text{eff}} = 6398$  K,  $\log g = 4.59$ , and the metal abundances described above, with the results of Runge-Kutta integrations performed by the Victoria evolutionary code. [A similar comparison (not shown) was carried out for a lower RGB model having  $T_{\text{eff}} = 5444$  K and  $\log g = 3.35$ : it looked qualitatively the same as Fig. 13.] As noted

previously, in connection with Fig. 1, which shows that much closer agreement is obtained in the case of a solar model, the differences between the solid and dashed curves are consistent with the expected consequences of the diffusion approximation.

However, it turns out that these differences do not have a significant effect on the predicted effective temperatures of stellar models, probably because the atmospheres are so thin that slight variations in the atmospheric structures give rise to no more than minor perturbations to the boundary conditions. Figure 14 shows that the tracks which are obtained for a  $0.8M_{\odot}$  star when MARCS model atmospheres are attached at the photosphere or at  $\tau = 100$  are essentially indistinguishable (compare the solid and dashed curves). Also plotted in this figure are evolutionary sequences for the same mass and chemical abundances, but assuming that the outer atmospheric temperature distributions are given by KS66 or gray  $T(\tau, T_{\text{eff}})$  relations. These calculations, which also assume the values of  $\alpha_{\text{MLT}}$  from the appropriately calibrated solar models (see Fig. 3), are both remarkably close to the tracks utilizing MARCS model atmospheres. Although one might be tempted to conclude from this that stellar models for very metal-poor stars do not have a very sensitive dependence on the treatment of the atmosphere, it must be kept in mind that the effects of differences in the assumed mixing-length parameters have conspired to produce the apparent similarity of the tracks that have been plotted.

Indeed, the small differences that exist are contrary to expectations. In particular, it seems odd that the main-sequence portions of the tracks that employ MARCS model atmospheres would be warmer than those using gray atmospheric structures, and that the gray and KS66 models would be nearly coincident, despite being based on very different  $T(\tau, T_{\text{eff}})$  relations. These anomalies have arisen because the respective values of  $\alpha_{\text{MLT}}$  that have been assumed are quite different. For instance, suppose that the models with gray atmospheres are recomputed on the assumption that  $\alpha_{\text{MLT}} = 2.0$ ; i.e., the same value of the mixing-length parameter that is needed to produce a Standard Solar Model when the KS66 atmospheres are assumed. If the models with gray atmospheres are revised in this way, a markedly different comparison between the different tracks is obtained, as shown in Figure 15.

Now the models with the gray atmospheres are appreciably hotter than those that describe the atmospheric layers using the KS66  $T(\tau, T_{\text{eff}})$  relation, and the tracks using MARCS atmospheres lie between them. This certainly corresponds more closely to one’s (possibly naive) expectations. However, a significantly warmer giant branch is not predicted by models that use MARCS SDC atmospheres (for  $[\text{Fe}/\text{H}] = -2.0$ ) as boundary conditions. As shown in Fig. 16, evolutionary sequences based on SDC atmospheres hardly differ from those employing KS66 or HM74 atmospheres. This is especially true at low  $Z$ , but even at

the solar metallicity, the differences between these cases are small. In other words, models having KS66 or HM74 atmospheres are able to reproduce the calculations based on MARCS SDC atmospheres rather well, nearly independently of the assumed metal abundance — which is a very surprising result!

Note that, for each of the four cases considered in Fig. 16,  $\alpha_{\text{MLT}}$  has been properly calibrated using the Sun. In fact, the differences in the assumed values of  $\alpha_{\text{MLT}}$  are largely responsible for the separations of the RGB loci: not only do the predicted temperatures at a given  $M_V$  tend to increase with increasing  $\alpha_{\text{MLT}}$  (as expected), but the shift in  $T_{\text{eff}}$  due to a given change in  $\alpha_{\text{MLT}}$  is much larger for metal-rich giants than for those of low  $Z$  (which is also consistent with expectations; see Fig. 3 by Vandenberg 1983). Had a constant value of the mixing-length parameter been assumed, the differences between the tracks would have been considerably smaller (but then, of course, the solar constraint would not have been satisfied equally well by the different calculations).

Two other points should be made concerning Fig. 16. First, the solar tracks represented by the dashed and dotted curves required slightly different values of  $\alpha_{\text{MLT}}$  to satisfy the solar constraint, even though both describe the upper atmosphere of the Sun using the HM74  $T(\tau, T_{\text{eff}})$  relation. However, the MARCS SDC atmospheres take macroturbulence into account, and as already noted in § 3.1.1, a slight reduction in the assumed value of  $\alpha_{\text{MLT}}$  is needed to compensate for this additional physics. Second, predicted temperatures have a fairly significant dependence on the fitting point that is adopted when MARCS SDC atmospheres are attached to interior models. This is not entirely unexpected because the temperature structures of these atmospheres (for the convective, sub-photospheric layers, in particular), being based on the empirical HM74 model for the Sun, may well be quite different from those predicted by the models that assume the mixing-length theory. Indeed, this may explain why the value of  $\alpha_{\text{MLT}}$  that is required by a Standard Solar Model must be changed from 1.94 to 2.01 when the SDC atmospheres are attached at the photosphere or at  $\tau = 5$ , respectively.

Despite this concern, the sequences of models having KS66 or HM74 atmospheres are remarkably similar to those using MARCS SDC atmospheres, both at the solar metallicity and at  $[\text{Fe}/\text{H}] = -2.0$ . Fig. 16 has certainly reinforced the indications from Fig. 6 that the variations in the predicted  $T$ - $\tau$  structures from model atmospheres encompassing wide ranges in the fundamental stellar parameters cannot be very large. This conjecture is corroborated by Figure 17, which compares the variations of  $(T/T_{\text{eff}})^4$  with  $\log \tau$  from MARCS SDC model atmospheres appropriate to giants and dwarfs having  $[\text{Fe}/\text{H}] = 0.0$  and  $-2.0$  with those given by the HM74 or gray  $T(\tau, T_{\text{eff}})$  relations. The similarity of the different loci between  $\log \tau \sim -4$  and  $\sim +0.2$  is striking. Only the gray atmosphere is offset from the

others by a moderately large amount — and because it is so discrepant from the predictions of proper model atmospheres, even for low  $[\text{Fe}/\text{H}]$  values, it seems inadvisable to use such atmospheres in deriving the surface boundary conditions of stellar models.

On the other hand, it is very encouraging that (i) the predicted  $T$ – $\tau$  relations from MARCS SDC atmospheres, throughout most of the line-forming region, are very robust, in the sense that changes to them arising from variations in the global properties of stars (i.e.,  $T_{\text{eff}}$ , surface gravity, and chemical composition) are small, and (ii) the HM74 solar atmosphere provides a reasonably good average of the model atmosphere predictions over a large region of parameter space. Thus, the commonly used practice of determining the photospheric pressure by integrating the hydrostatic equation in conjunction with a scaled-solar  $T(\tau, T_{\text{eff}})$  relation (either KS66 or HM74) has much to commend it. Indeed, the differences between evolutionary calculations that employ KS66 or HM74 atmospheres and those based on the more sophisticated MARCS SDC model atmospheres are probably too small to be observationally detectable, given current uncertainties in the measured properties of stars. To amplify on this point, we now turn to some comparisons of our isochrones for  $[\text{Fe}/\text{H}] = -2.0$  with the observed CMD of the globular cluster M 68, which has  $[\text{Fe}/\text{H}] = -1.99 \pm 0.06$ , according to the results of high-resolution spectroscopy carried out by Carretta & Gratton (1997).

#### 4.1. Fits of Isochrones to the CMD of M 68

The giant and subgiant sequences of M 68 are especially well defined in the “standard field” photometry provided by Stetson (2000);<sup>6</sup> consequently, we have opted to use these data to determine the mean locus describing the evolved stars. Stetson’s observations and our eye-estimated, hand-drawn curve through them are plotted in Figure 18. The solid curve merges smoothly into the fiducial that Vandenberg (2000) used to represent the stars fainter than  $V = 19$  in the deep CMD obtained by Walker (1994). In this way, a CMD has been obtained for M 68 that extends from  $\sim 4.5$  mag above the cluster turnoff to  $\sim 3.5$  mag below it.

Grids of evolutionary tracks were computed on the assumption that the pressure at the photosphere was obtained (i) from fully consistent (standard) MARCS model atmospheres, which may be fine for metal-deficient stars even though they have some short-comings in reproducing solar observations, and (ii) by integrating the equation of hydrostatic equilibrium on the assumption of the KS66  $T(\tau, T_{\text{eff}})$  relation. (Only these two cases are considered

---

<sup>6</sup>See <http://cadwww.hia.nrc.ca/standards>.

because the low-metallicity tracks that were computed for the different treatments of the atmosphere are so similar; see Figs. 14 and 16. Note, in particular, that the evolutionary sequence which made use of MARCS SDC atmospheres tends to lie on or between those for the above two cases.) Needless to say, the calibrated values of  $\alpha_{\text{MLT}}$  from the respective Standard Solar Models were adopted.

Isochrones for ages of 12, 14, and 16 Gyr were derived by interpolation in the tracks, and then they were transposed to the observed plane using the  $(V - I) - T_{\text{eff}}$  relations given by VandenBerg & Clem (2003). If the reddening implied by the Schlegel et al. (1998) dust maps is assumed, and the apparent distance modulus is determined by main-sequence fits to the isochrones, we obtain the comparisons between theory and observations shown in Figure 19. The fit to the observations in the upper panel is quite agreeable, aside from a slight offset between the isochrones and the cluster fiducial at  $M_V \lesssim 0.0$ , which suggests that there is a minor problem with the predicted temperatures or colors for metal-poor giants. (Note that the indicated age,  $\approx 14.5$  Gyr, would be reduced by  $\sim 10\text{--}12\%$  if diffusive processes were taken into account; see VandenBerg et al. 2002.)

Because the ZAMS for the models using KS66 atmospheric structures is cooler than that based on MARCS model atmospheres, this case (see the lower panel in Fig. 19) leads to a somewhat larger distance modulus, a younger age, and a more pronounced discrepancy along the giant branch. To demonstrate the sensitivity of the model fits to a change in the assumed distance, zero-age horizontal branch (ZAHB) loci were computed on the assumption of the envelope helium abundance and core mass given by a  $0.8M_{\odot}$  model when the He-burning luminosity (at the tip of the RGB) had surpassed  $100 L_{\odot}$ . (A ZAHB model was calculated according to the standard procedure whereby an initial structure for a given mass was constructed to have the helium core mass and envelope chemical abundance profiles from a suitable giant-branch precursor, and then relaxed over many short time steps until it attained an age of 2 Myr. The 20–30 models that constitute a ZAHB locus were produced by successively reducing the envelope mass, while maintaining a fixed core mass.)

If the distance to M 68 is derived by fitting the sample of cluster horizontal-branch stars observed by Walker (1994) to this ZAHB, one obtains  $(m - M)_V = 15.26$ .<sup>7</sup> To identify

---

<sup>7</sup>VandenBerg & Clem (2003) previously found  $(m - M)_V = 15.18$  using the ZAHB locus computed by VandenBerg et al. (2000) for  $[\text{Fe}/\text{H}] = -2.01$  and  $[\alpha/\text{Fe}] = 0.3$ . Approximately 0.06 mag of the difference is due to the assumption, in the present ZAHB models, of a higher helium content and a slightly larger core mass, which is a consequence of using the conductive opacities by Potekhin et al. (1999) instead of those by Hubbard & Lampe (1969). The remainder can be attributed to the change made by VandenBerg et al. (2006) to the VandenBerg & Clem bolometric corrections so that  $M_{V,\odot} = 4.82$  instead of 4.84. Since the VandenBerg et al. (2000) ZAHB loci were found to be  $\sim 0.02$  mag fainter than the empirical estimates

which isochrone provides the best match to the observed CMD in the vicinity of the turnoff, it is necessary to adjust the isochrones to the red by 0.026 mag and 0.013 mag in order that the MARCS and KS66 atmosphere-interior models for the unevolved stars, respectively, reproduce the observed ZAMS. The results of this exercise are shown in Figure 20: the inferred age of M 68 (which is independent of the treatment of the atmosphere, as it should be) is close to 12 Gyr.

The main difficulty with this interpretation of the observed CMD is the large discrepancy between the predicted and observed giant branch loci, which was obviously exacerbated by the adopted redward color shift. However, this problem would disappear if the giant-branch segments of the isochrones were hotter by only  $\delta \log T_{\text{eff}} = 0.01$ . This is demonstrated by the dashed curves in Fig. 20, which indicate where the RGBs of the 12 Gyr isochrones would be located if the model temperatures were increased by this amount (assuming the same color transformations that were used for the solid curves; i.e., those by Vandenberg & Clem 2003). Since the giant branches that are plotted in Fig. 15 for the gray and KS66 cases differ in temperature, at a given luminosity, by only  $\delta \log T_{\text{eff}} \approx 0.015$ , it is easily possible that the assumed distance in Fig. 20 is accurate and that the giant-branch discrepancies have arisen mainly because the model temperatures are too low by  $\approx 100$  K.

However, there may well be other contributing factors. For instance, the color transformations by Vandenberg & Clem (2003), which we have used here, may be too red for low gravity stars; though this seems unlikely because they are essentially identical with those predicted by Bell & Gustafsson (1989), which satisfy a number of observational constraints, and because the majority of alternative color– $T_{\text{eff}}$  relations (by, e.g., Castelli 1999; Lejeune, Cuisinier, & Buser 1998) are even redder (see the comparison plots provided by Vandenberg & Clem). It may also be the case that the adopted metallicity of M 68 is too high. Kraft & Ivans (2003) have obtained  $[\text{Fe}/\text{H}] \approx -2.4$  for this system using high-resolution spectroscopy, but relying on Fe II lines instead of Fe I lines, which were the basis of the metallicity determinations by Carretta & Gratton (1997). In this regard, Asplund (2004) has concluded from his 3-D, LTE calculations that abundances derived from minority species (like Fe I) will be over-estimated by  $\gtrsim 0.3$  dex if 1-D model atmospheres (which were used by both Kraft & Ivans and Carretta & Gratton) are employed in the analysis. According to Asplund, “it is clear that globular cluster metallicities should be based on Fe II lines”. As is well known, stellar models for lower metallicities have hotter giant branches if all other parameters are kept the same.

---

of RR Lyrae luminosities by De Santis & Cassisi (1999) and Cacciari, Corwin, & Carney (2005), the ZAHB used in this study to provide the lower bound to the distribution of HB stars in M 68 is brighter than these determinations by  $\sim 0.06$  mag.

If anything, the models for metal-poor main-sequence stars are too hot/blue, due to the fact that they do not take diffusive processes into account. However, models with uninhibited diffusion are ruled out by the observed Li abundances in low-metallicity field turnoff stars (the Spite plateau; see Richard et al. 2002) and the smaller-than-expected variation in the abundances of heavy elements between the turnoff and the lower RGB in NGC 6397 (Korn et al. 2006). These constraints can be satisfied if turbulent mixing below convective envelopes is invoked, which has the additional consequence that the predicted temperatures at the turnoffs of isochrones, where the effects of diffusion are most pronounced, do not differ by more than  $\approx 60$  K from those given by non-diffusive models (see the plots provided by Vandenberg et al. 2002). It is difficult to say how this result would be altered if fully consistent model atmospheres were used as boundary conditions. This should be explored, though such a project would be computationally demanding because small grids of model atmospheres would have to be calculated along each evolutionary track to follow the surface abundance variations arising from the combined effects of gravitational settling, radiative accelerations, and turbulent mixing.

Although our analysis of M 67 giants suggested that  $\alpha_{\text{MLT}}$  does not vary with  $T_{\text{eff}}$  or  $\log g$ , it is clear from the above discussion that the many uncertainties at play in the case of the globular cluster M 68 make it impossible to say whether or not the mixing-length parameter varies either with  $[\text{Fe}/\text{H}]$  or with evolutionary state within a metal-deficient system.

## 5. Conclusions

This investigation has been carried out to examine the consequences for stellar models of using fully consistent MARCS model atmospheres to describe their outer layers and to explore how such models differ from those that base the determination of the photospheric pressure on either the classical gray or KS66  $T(\tau, T_{\text{eff}})$  relationship. Nearly all large grids of stellar models computed to date have opted for the latter approach, which must lead to systematic errors in the predicted  $T_{\text{eff}}$  scale, since the same  $T$ - $\tau$  structure (scaled to the relevant value of  $T_{\text{eff}}$ ) cannot apply to stars in all parts of the H-R diagram. One would expect that the use of proper model atmospheres to determine the boundary conditions of stellar models would result in effective temperatures that are systematically more correct.

Solar abundance models that describe the atmosphere using the KS66  $T(\tau, T_{\text{eff}})$  relation predict considerably warmer giant branches than those using MARCS or gray atmospheres, and in fact, the application of the latest  $(V - K)$ - $T_{\text{eff}}$  relations to giants in the  $[\text{Fe}/\text{H}] \approx 0.0$  open cluster M 67 suggest that the hotter temperatures are the most accurate ones. This study has shown that the impact of the diffusion approximation for describing the radiative

transfer in stellar interior models is inconsequential (at least for solar-type stars), insofar as nearly the same tracks are obtained whether MARCS atmospheres, which obtain “exact” solutions to the transfer equation, are attached at the photosphere or at  $\tau = 100$ . The higher temperatures that are obtained when scaled solar model atmospheric structures are assumed arise because the solar model for this case requires  $\alpha_{\text{MLT}} = 2.00$ , whereas the solar model with a MARCS atmosphere requires  $\alpha_{\text{MLT}} = 1.80$ . The failure of current 1-D model atmospheres to reproduce the actual temperature structure of the Sun is undoubtedly contributing to some (perhaps most) of the differences between the tracks using MARCS and scaled solar atmospheres as boundary conditions.

Stellar models with gray atmospheres can hardly be expected to be representative of metal-rich stars like the Sun, nor does it make any sense that such models for giant stars predict cooler effective temperatures than those using the KS66  $T(\tau, T_{\text{eff}})$  relation to describe the atmospheric layers. And yet, this is precisely what happens when the two sets of models are made to satisfy the solar constraint by setting the value of  $\alpha_{\text{MLT}}$  appropriately. (The best estimate of  $\alpha_{\text{MLT}}$  is obviously the value obtained when an empirical solar atmosphere is used in the calculation of a Standard Solar Model, not a gray atmosphere.) It is perhaps more reasonable to expect that gray atmospheres would be most relevant for models of very metal-deficient stars, but how realistic is such an assumption? To investigate this question, as well as the issues discussed in the previous paragraph, “scaled solar, differentially corrected” (SDC) MARCS atmospheres were constructed that yield the empirical  $T$ - $\tau$  structure of the Sun (specifically that derived by HM74, which is an improvement over the earlier KS66 description) if solar parameters are assumed, and yet retain the differential effects on the  $T(\tau, T_{\text{eff}})$  relations that are predicted by theoretical MARCS atmospheres for different values of  $T_{\text{eff}}$ ,  $\log g$ , and metallicity.

It is certainly a most interesting and important result of this study that the temperature structures of these SDC atmospheres, from  $\tau \sim 10^{-4}$  to  $\tau \sim 1$ , are rather weak functions of the basic stellar parameters, and that, in the mean, they are well reproduced by the HM74 (or KS66)  $T(\tau, T_{\text{eff}})$  relations. As a result, stellar models that use SDC atmospheres as boundary conditions satisfy the solar constraint on the assumption of  $\alpha_{\text{MLT}} \approx 2.0$  (by design) and they reproduce the temperatures of M67 giants just as well as the models employing KS66 atmospheres. Moreover, the differences between the tracks with these two treatments of the atmospheric layers are in very good agreement at  $[\text{Fe}/\text{H}] = -2.0$  as well. (Even at this metallicity, gray atmospheres are not good approximations to proper model atmospheres.)

However, it is not necessarily the case that SDC atmospheres represent those of metal-deficient stars better than standard MARCS models just because the latter are problematic

for metal-rich dwarfs. Furthermore, while the MARCS models (including the SDC version) treat the changing character of the radiative energy transfer as the distribution of opacity varies with fundamental stellar parameters, the energy balance may well be qualitatively different in real stellar atmospheres, as compared with the predictions of mixing-length models, due to variations in the convective fluxes in the outer layers. Thus, if the differential effects of convection for stars of different  $T_{\text{eff}}$ , surface gravity, and metallicity are considerable, they may offset or even counteract the effects calculated by models (such as ours) that are in radiative equilibrium in the visible layers. It would be just fortuitous if, for instance, those convection effects were such that the scaled solar atmospheres (i.e., HM74 or KS66) were closest to the true structure. As far as the choice between SDC and standard MARCS models is concerned, it seems clear that, for stars having close to solar parameters, the SDC models are to be preferred. Fortunately, both SDC and standard MARCS atmospheres imply quite similar  $T_{\text{eff}}$  scales for metal-poor stars (if  $\alpha_{\text{MLT}}$  is obtained from the respective Standard Solar Model).

We thank Santi Cassisi for a very thoughtful and helpful report on this paper. This work has been supported by the Natural Sciences and Engineering Research Council of Canada through a Discovery Grant to DAV, and by grants from the Swedish Research Council to BE, KE, and BG.

## REFERENCES

- Asplund, M. 2004, in Proceedings of JD4 at the XXIII IAU General Assembly: Astrophysical Impact of Abundances in Globular Clusters, eds. F. D'Antona & G. Da Costa, Mem. Soc. Astron. Ital., 75, 300.
- Asplund, M., Grevesse, N., & Sauval, A. J. 2006, Comm. in Asteroseismology, 147, 76.
- Asplund, M., Grevesse, N., Sauval, S. J., Allende Prieto, C., & Blomme, R. 2005, A&A, 431, 693.
- Asplund, M., Nordlund, A., & Trampedach, R. 1999, In Theory and Tests of Convection in Stellar Structure, eds. A. Giménez, E. F. Guinan, & B. Montesinos, ASP Conf. Ser., 173, 221.
- Baraffe, I., Chabrier, G., Allard, F., & Hauschildt, P. H. 1997, A&A, 327, 1054.
- Bell, R. A., & Gustafsson, B. 1989, MNRAS, 236, 653.
- Bessell, M. S., & Brett, J. M. 1988, PASP, 100, 1134.
- Bessell, M. S., Castelli, F., & Plez, B. 1998, A&A, 333, 231.
- Blackwell, D. E., Lynas-Gray, A. E., & Smith, G. 1995, A&A, 296, 217.
- Böhm-Vitense, E. 1958, Zs. Ap., 46, 108.
- Brocato, E., Cassisi, S., & Castellani, V. 1998, MNRAS, 295, 711.
- Cacciari, C., Corwin, T. M., & Carney, B. W. 2005, AJ, 129, 267.
- Carretta, E., & Gratton, R. G. 1997, A&AS, 121, 95.
- Cassisi, S., Salaris, M., Castelli, F., & Pietrinferni, A. 2004, ApJ, 616, 498.
- Castelli, F. 1999, A&A, 346, 564.
- Cayrel, R., et al. 2004, A&A, 416, 1117.
- Coc, A., Vangioni-Flam, E., Descouvemont, P., Adahchour, A., & Angulo, C. 2004, ApJ, 600, 544.
- Collet R., Asplund M., & Trampedach R. 2007, astro-ph/0703652.
- De Santis, R., & Cassisi, S. 1999, MNRAS, 308, 97.

- Ferguson, J. W., Alexander, D. R., Allard, F., Barman, T., Bodnarik, J. G., Hauschildt, P. H., Heffner-Wong, A., & Tamani, A. 2005, *ApJ*, 623, 585.
- Ferraro, F. R., Valenti, E., Straniero, O., & Origlia, L. 2006, *ApJ*, 642, 225.
- Girardi, L., Bressan, A., Bertelli, G., & Chiosi, C. 2000, *A&AS*, 141, 371.
- Grevesse, N., & Noels, A. 1993, *Phys. Scr.*, T47, 133.
- Grevesse, N., & Sauval, A. J. 1998, *Space Sci. Rev.*, 85, 161. (GS98)
- Gustafsson, B., Bell, R. A., Eriksson, K., & Nordlund, A. 1975, *A&A*, 42, 407.
- Gustafsson, B., Edvardsson, B., Eriksson, K., Mizuno-Wiedner, M., Jorgensen, U. G., & Plez, B. 2003, in *Stellar Atmosphere Modelling*, eds. I. Hubeny, D. Mihalas, & K. Werner, *ASP Conf. Ser.*, 288, 331.
- Henry, L. G., Forbes, J. E., & Gould, N. L. 1964, *ApJ*, 139, 306.
- Heiter, U., & Eriksson, K. 2006, *A&A*, 452, 1039.
- Henry, L., Vardya, M. S., & Bodenheimer, P. 1965, *ApJ*, 142, 841.
- Hobbs, L. M., & Thorburn, J. A. 1991, *AJ*, 102, 1070.
- Holweger, H., & Müller, E. A. 1974, *Solar Phys.*, 39, 19. (HM74)
- Houdashelt, M. L., Bell, R. A., & Sweigart, A. V. 2000, *AJ*, 119, 1448.
- Houdashelt, M. L., Frogel, J. A., & Cohen, J. G. 1992, *AJ*, 103, 163.
- Hubbard, W. B., & Lampe, M. 1969, *ApJS*, 18, 297.
- Iglesias, C. A., & Rogers, F. J. 1996, *ApJ*, 464, 943.
- Irwin, A. W. 1985, *A&A*, 146, 282.
- Kippenhahn, R., Weigert, A., & Hofmeister, E. 1967, in *Methods of Computational Physics*, vol. 7, eds. B. Alder, S. Fernbach, & M. Rotenberg (New York: Academic), p. 129.
- Korn, A. J., Grundahl, F., Richard, O., Barklem, P. S., Mashonkina, L., Collet, R., Piskunov, N., & Gustafsson, B. 2006, *Nature*, 442, 657.
- Kraft, R. P., & Ivans, I. I. 2003, *PASP*, 115, 143.
- Krishna Swamy, K. S. 1966, *ApJ*, 145, 174. (KS66)

- Lejeune, T., Cuisinier, F., & Buser, R. 1998, *A&AS*, 130, 65.
- Ludwig, H.G., Freytag, B., & Steffen, M. 1999, *A&A*, 346, 111.
- Mihalas, D. 1970, *Stellar Atmospheres* (San Francisco: W. H. Freeman).
- Montalbán, J., Kupka, F., D’Antona, F., & Schmidt, W. 2001, *A&A*, 370, 982.
- Montgomery, K. A., Marschall, L. A., & Janes, K. A. 1993, *AJ*, 106, 181.
- Morel, P., van’t Meer, C., Provost, J., Berthomieu, G., Castelli, F., Cayrel, R., Goupil, M. J., & Lebreton, Y. 1994, *A&A*, 286, 91.
- Pedersen, B. B., VandenBerg, D. A., & Irwin, A. W. 1990, *ApJ*, 352, 279.
- Pietrinferni, A., Cassisi, S., Salaris, M., & Castelli, F. 2004, *ApJ*, 612, 168.
- Potekhin, A. Y., Baiko, D. A., Haensel, P., & Yakovlev, D. G. 1999, *A&A*, 346, 345.
- Randich, S., Sestito, P., Primas, F., Pallavicini, R., & Pasquini, L. 2006, *A&A*, 450, 557.
- Richard, O., Michaud, G., Richer, J., Turcotte, S., Turck-Chiéze, & VandenBerg, D. A. 2002, *ApJ*, 568, 979.
- Rood, R. T., & Crocker, D. A. 1985, in *Production and Distribution of C, N, O Elements*, eds. I. J. Danziger, F. Matteucci, & K. Kjær (Garching: ESO), p. 61.
- Salaris, M., Cassisi, S., & Weiss, A. 2002, *PASP*, 114, 375.
- Schlegel, D. J., Finkbeiner, D. P., & Davis, M. 1998, *ApJ*, 500, 525.
- Sekiguchi, M., & Fukugita, M. 2000, *AJ*, 120, 1072.
- Stetson, P. B. 2000, *PASP*, 112, 925.
- Tautvaišienė, G., Edvardsson, B., Tuominen, I., & Ilyin, I. 2000, *A&A*, 360, 499.
- van Belle, G. T., et al. 1999, *AJ*, 117, 521.
- VandenBerg, D. A. 1983, *ApJS*, 51, 29.
- VandenBerg, D. A. 1991, in *ASP. Conf. Ser. 13, The Formation and Evolution of Star Clusters*, ed. K. Janes (San Francisco: ASP), 183.
- VandenBerg, D. A. 1992, *ApJ*, 392, 685.

VandenBerg, D. A. 2000, ApJS, 129, 315.

VandenBerg, D. A., Bergbusch, P. A., & Dowler, P. D. 2006, ApJS, 162, 375.

VandenBerg, D. A., & Clem, J. L. 2003, AJ, 126, 778.

VandenBerg, D. A., Gustafsson, B., Edvardsson, B., Eriksson, K., & Ferguson, J. 2007, ApJL, submitted.

VandenBerg, D. A., & Poll, H. E. 1989, AJ, 98, 1451.

VandenBerg, D. A., Richard, O., Michaud, G., & Richer, J. 2002, ApJ, 571, 487.

VandenBerg, D. A., Swenson, F. J., Rogers, F. J., Iglesias, C. A., & Alexander, D. R. 2000, ApJ, 532, 430.

Walker, A. R. 1994, AJ, 108, 555.

Yi, S., Demarque, P., Kim, Y.-C., Lee, Y.-W., Ree, C. H., Lejeune, T., & Barnes, S. 2001, ApJS, 136, 417.

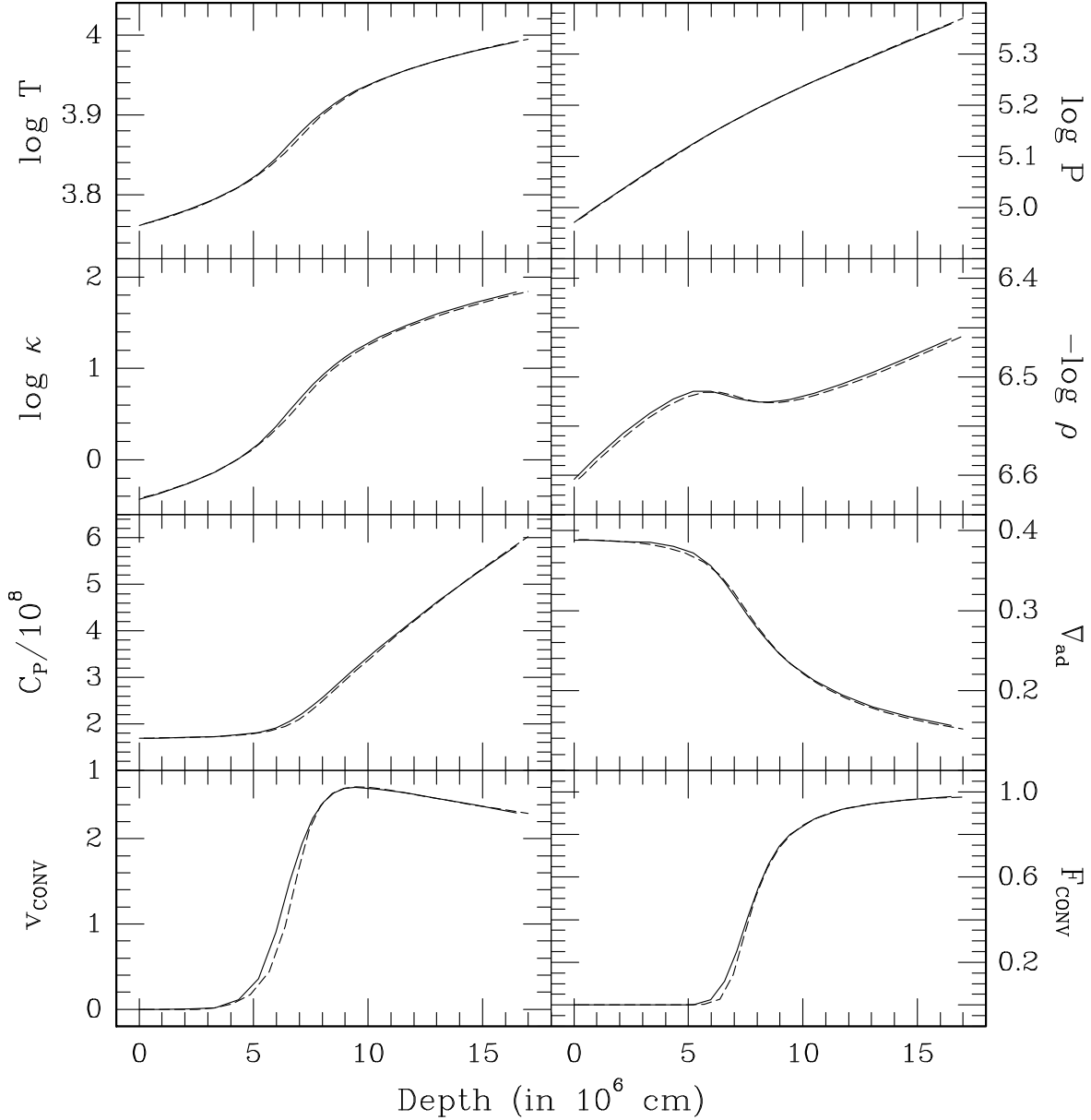


Fig. 1.— Comparison of various thermodynamic quantities ( $T$ ,  $P$ ,  $\rho$ ,  $C_P$ ,  $\nabla_A$ ), the opacity ( $\kappa$ ), the convective velocity ( $v_{\text{conv}}$ ), and the fraction of the total flux that is carried by convection ( $F_{\text{conv}}$ ) in the sub-photospheric layers of a solar model, as predicted by the MARCS atmosphere and Victoria stellar interior codes (solid and dashed curves, respectively), on the assumption of the Asplund heavy-element mixture (see Table 1). Both calculations assume  $\alpha_{\text{MLT}} = 1.80$ .

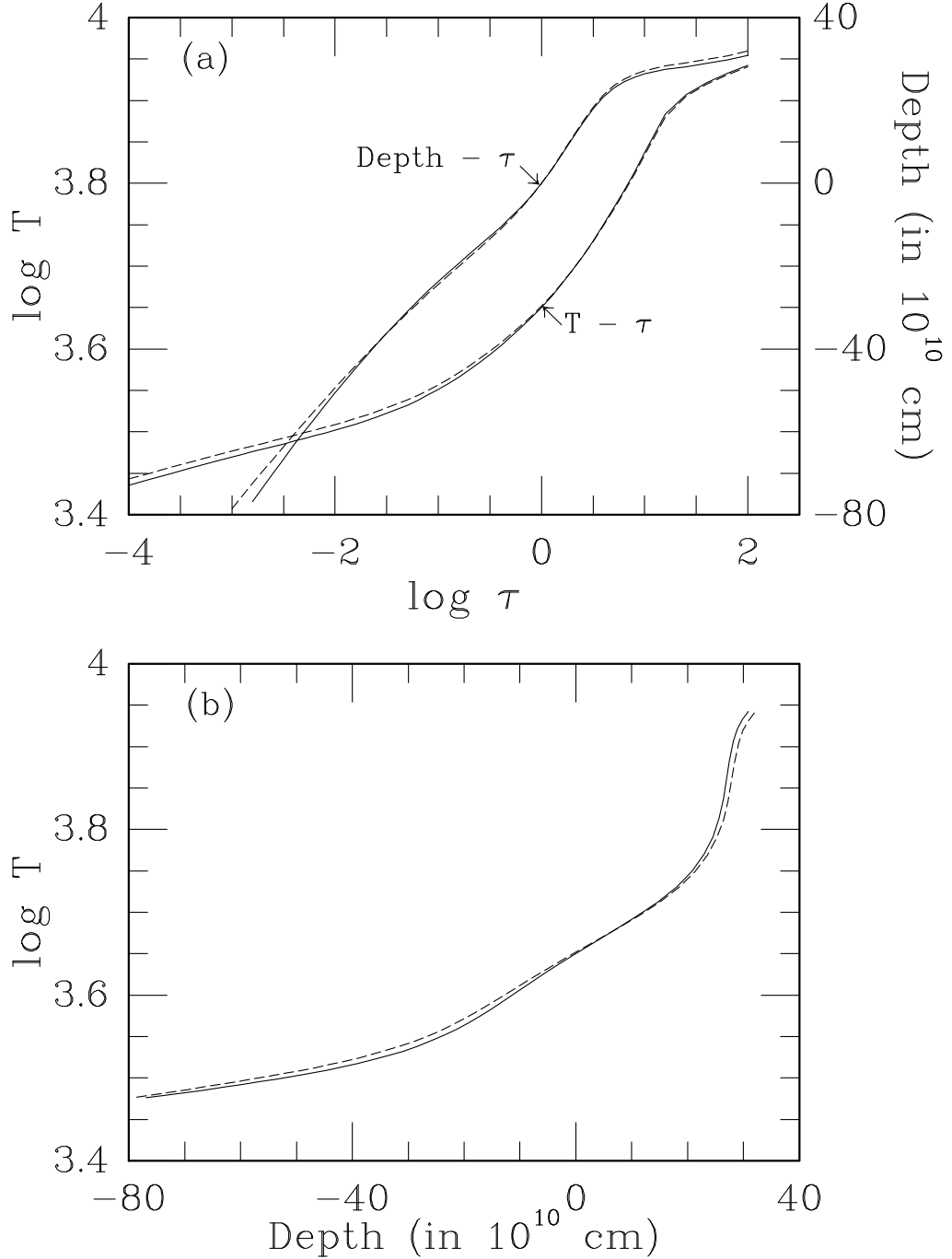


Fig. 2.— The variations of  $T$  and geometrical depth with  $\tau$  (upper panel) and of  $T$  with depth (lower panel) from spherical model atmospheres for stars having  $T_{\text{eff}} = 4000$  K,  $\log g = 0.0$ ,  $Z = 0.05$ , and masses of  $0.5 M_{\odot}$  (solid curves) and  $5.0 M_{\odot}$  (dashed curves), respectively. Note that the depth zero-point has been arbitrarily chosen to coincide with that layer where  $\tau = 1.0$ .

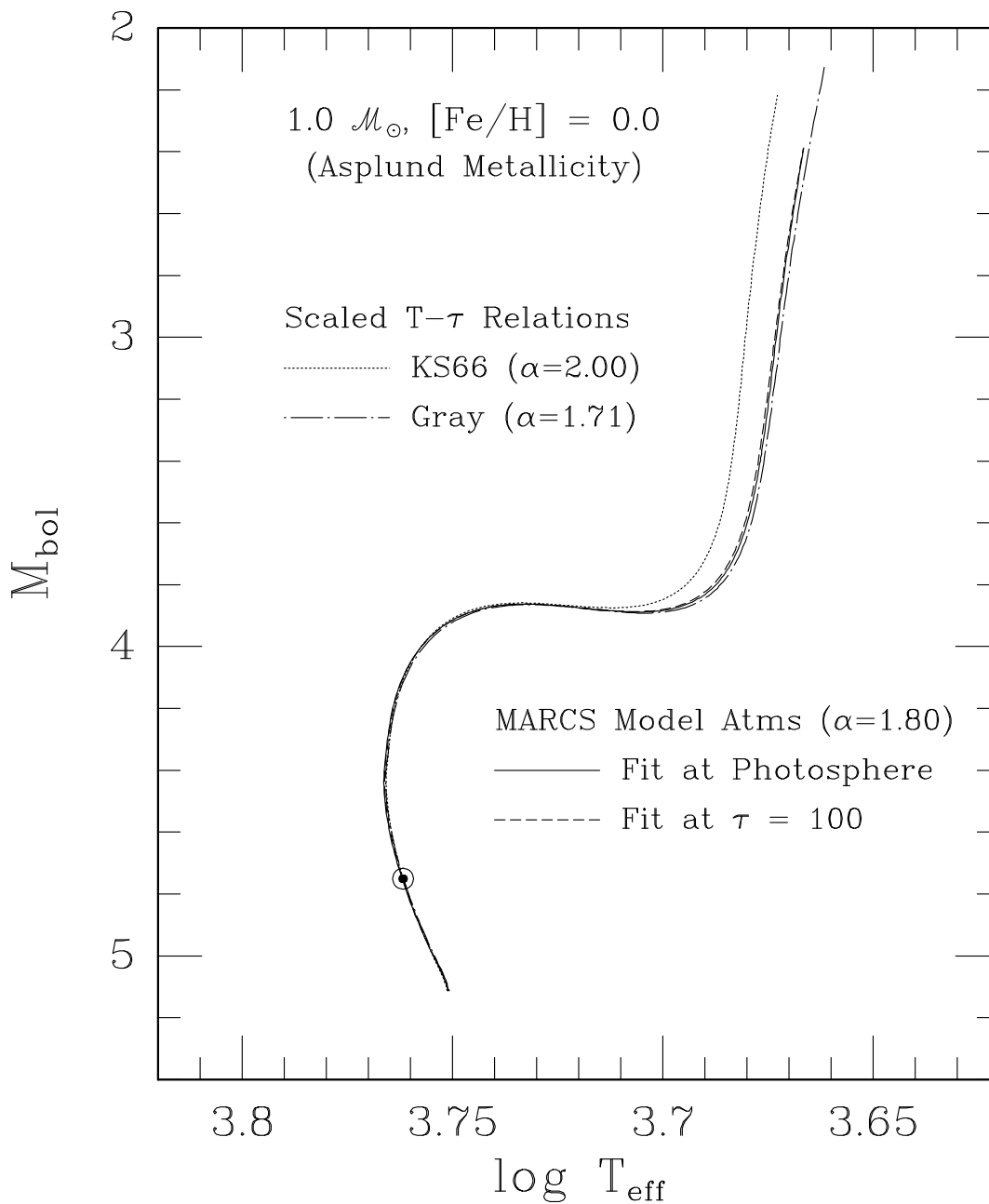


Fig. 3.— Plot on the H-R diagram of evolutionary tracks for  $1.0\mathcal{M}_{\odot}$  stellar models having  $Y = 0.257578$  and the Asplund heavy-element abundances (see Tables 1 and 2) with different treatments of the atmospheric layers, as indicated. In order for each case to satisfy the solar constraint (note the location of the solar symbol), the mixing-length parameter had to be set to the specified values.

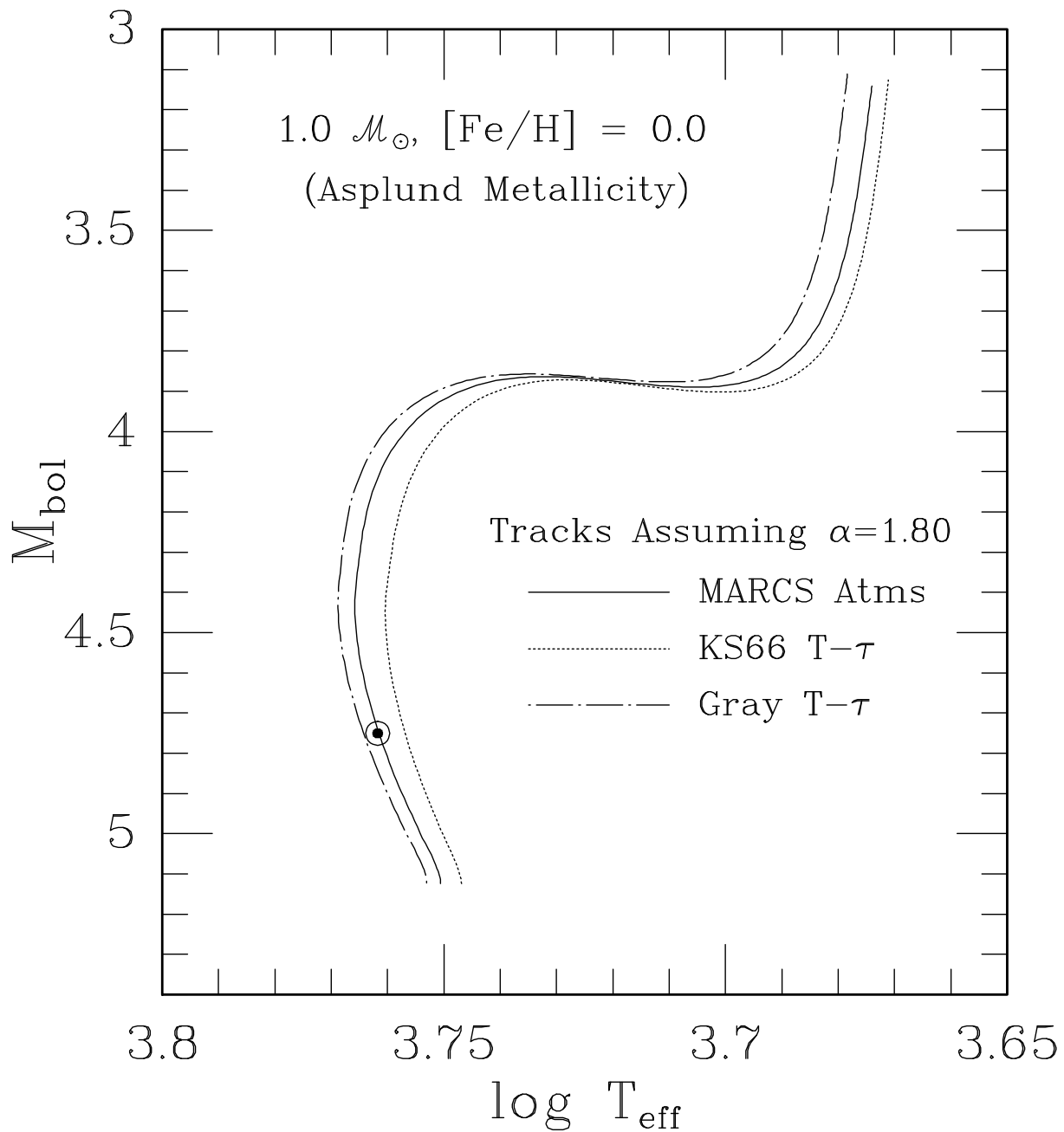


Fig. 4.— Similar to the previous figure, except that the tracks for the different treatments of the atmospheric layers all assume  $\alpha_{\text{MLT}} = 1.80$ . Since the tracks using MARCS atmospheres differ only slightly when attached at the photosphere or at  $\tau = 100$ , only the former case is plotted here.

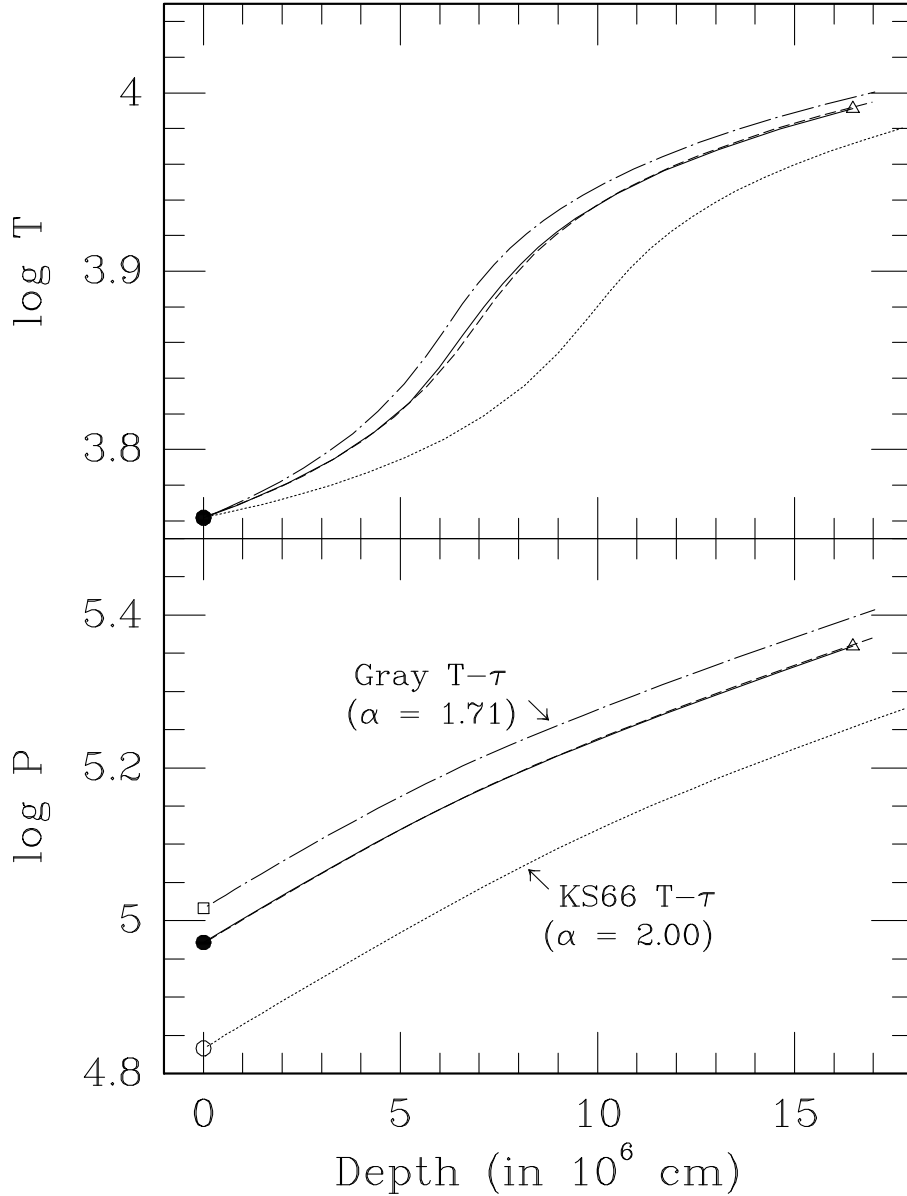


Fig. 5.— Plot of the variations of  $T$  and  $P$  with geometrical depth in the sub-photospheric layers of Standard Solar Models. (In this and similar plots, the depth is defined to be zero at the photosphere.) The solid curve represents a MARCS model atmosphere for the Sun. The dashed, dot-dashed, and dotted curves indicate the results of Runge-Kutta integrations (see the text) in which the initial value of  $T$  is the observed  $T_{\text{eff}}$  of the Sun and the initial values of  $P$  were obtained from the MARCS model or by integrating the hydrostatic equation for the gray or KS66  $T(\tau, T_{\text{eff}})$  relations, respectively. The solid and dashed curves both assume  $\alpha_{\text{MLT}} = 1.80$ : the adopted mixing-length parameters for the other two cases are as indicated. The symbols attached to the various curves provide identifications for the integrations to deeper layers that are plotted in Figure 7: one of these integrations begins at the location of the open triangle, which indicates the layer in the MARCS solar atmosphere where  $\tau = 100$ .

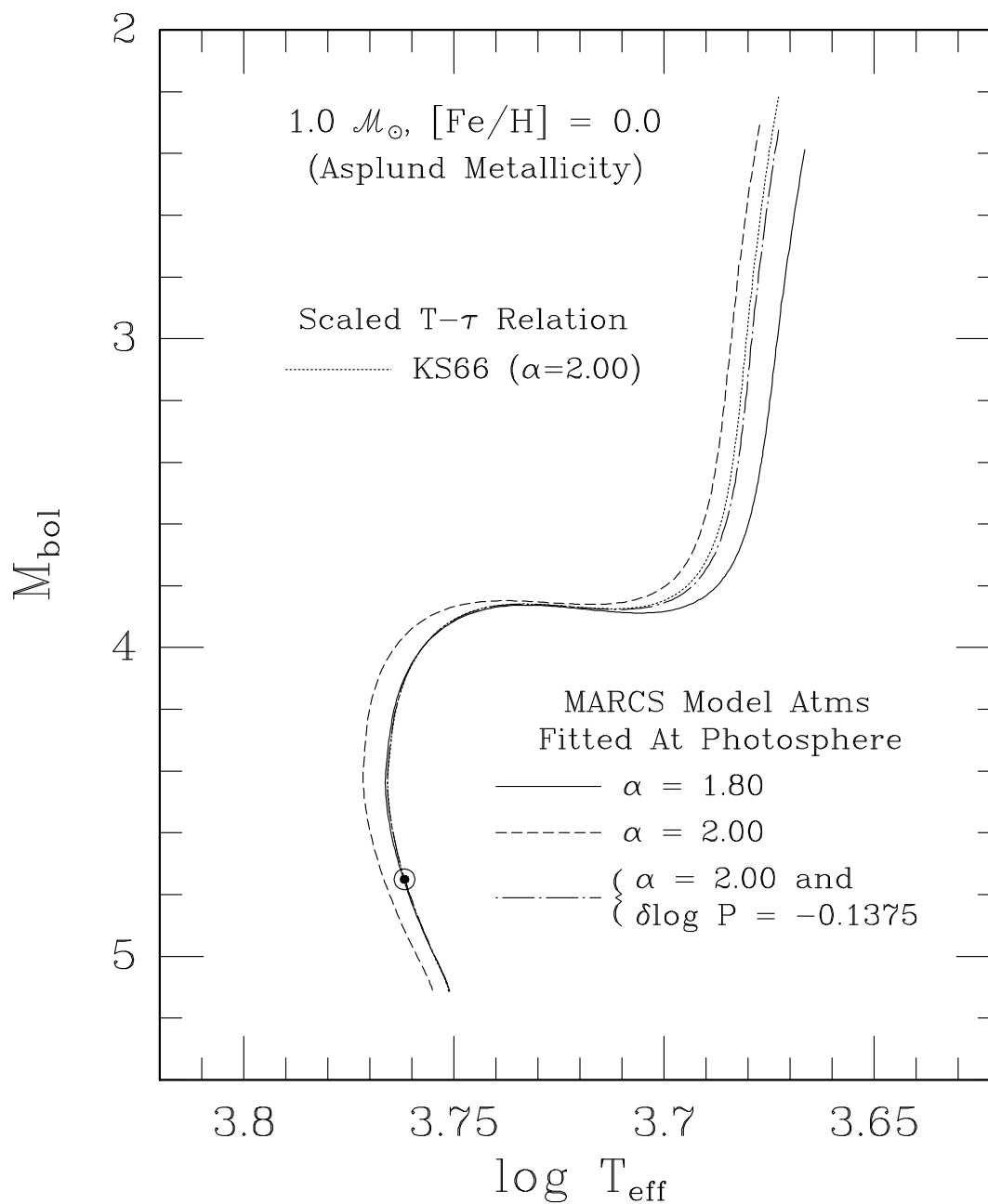


Fig. 6.— Similar to Fig. 3, except that the effects on the tracks of increasing  $\alpha_{\text{MLT}}$  from 1.80 to 2.00, and of adjusting the photospheric pressures predicted the MARCS atmospheres for  $\alpha_{\text{MLT}} = 2.0$  by  $\delta \log P = -0.1375$  are shown. Both the dotted and solid curves are identical to their counterparts in Fig. 3.

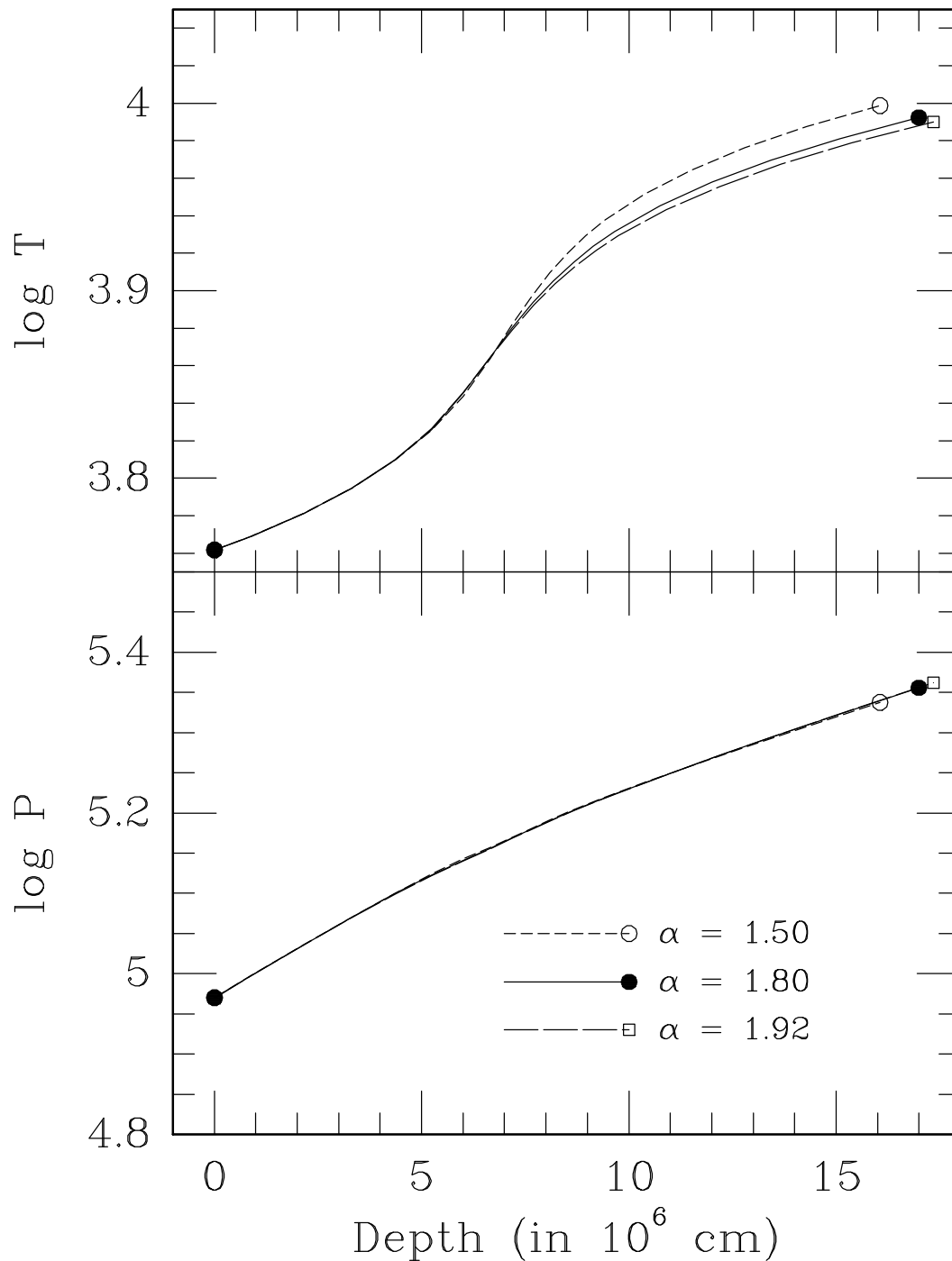


Fig. 7.— The variations of  $\log T$  and  $\log P$  with depth between the photosphere and that layer where  $\tau = 100$  from MARCS model atmospheres for  $\log g = 4.44$ ,  $T_{\text{eff}} = 5777$  K, Asplund abundances, and the three indicated values of  $\alpha_{\text{MLT}}$ . The solid curve plotted here is the same as the solid curve plotted in the previous figure.

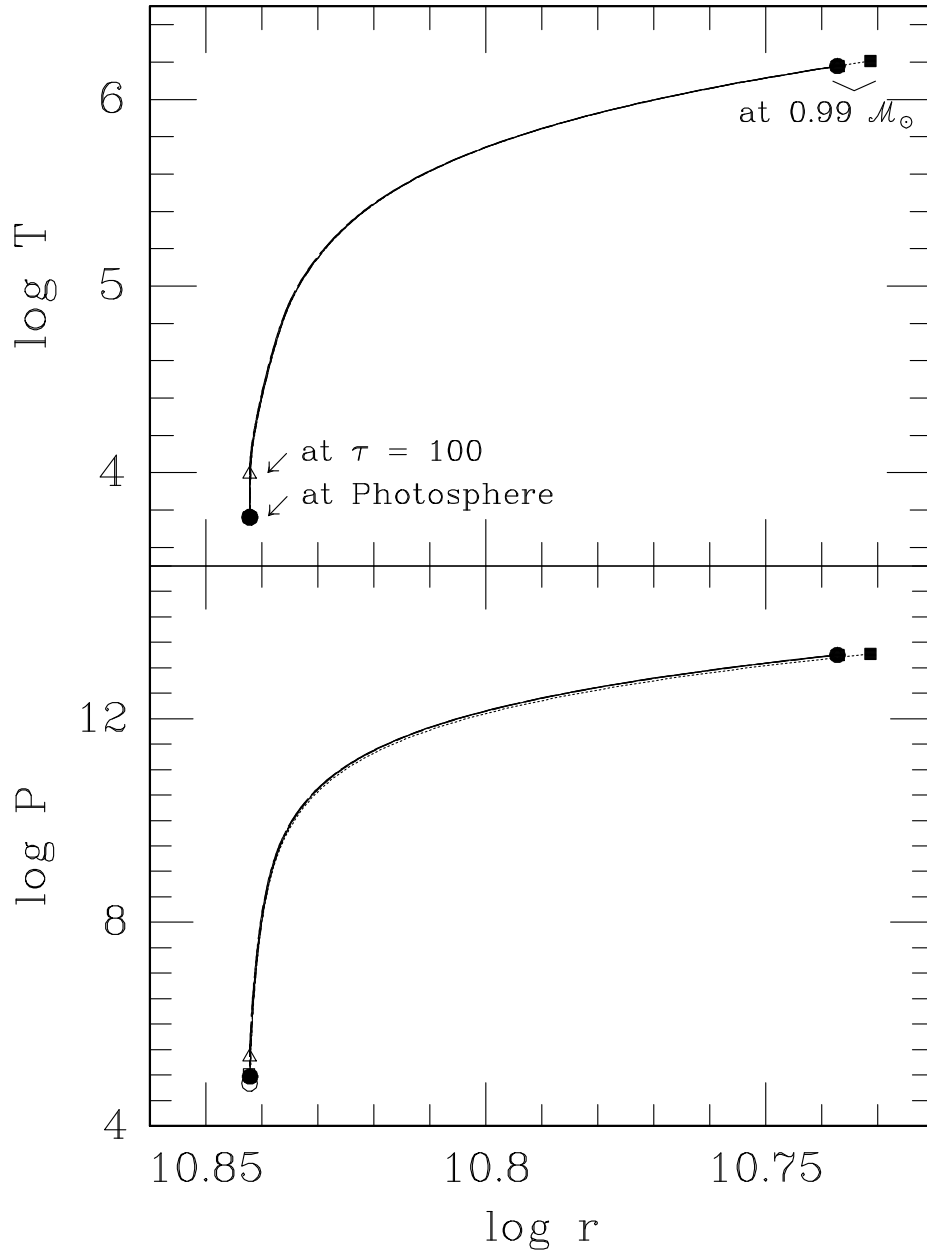


Fig. 8.— Similar to Fig. 5, except that the Runge-Kutta integrations are extended to  $0.99M_{\odot}$  (where the outer boundary conditions used to solve the stellar structure equations are defined; see the text). The symbols, which identify the same cases presented in Fig. 5, are plotted at both the beginning and end-points of the integrations: most are not visible because they superimpose one another. The dotted curve and filled square were obtained by repeating the integration represented by the long-dashed curve and filled circle plotted in Fig. 5, but assuming  $\alpha_{\text{MLT}} = 1.71$  instead of 1.80.

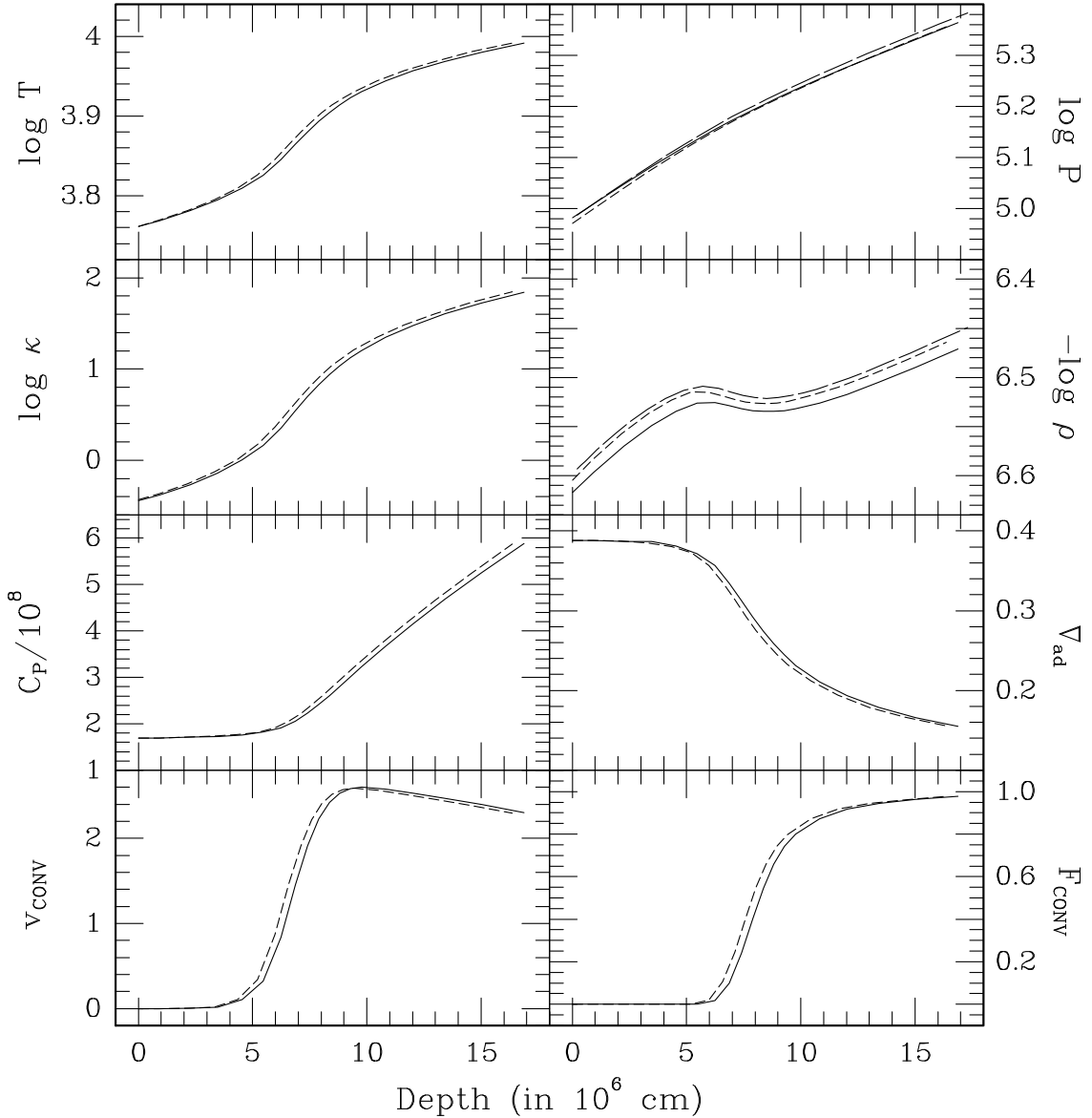


Fig. 9.— Similar to Fig. 1; in this case, the predictions from MARCS model atmospheres, with and without taking macroturbulence into account (solid and dashed curves, respectively) are compared. Long-dashed curves in the pressure-depth and density-depth panels indicate the results of Runge-Kutta integrations inward from the photosphere with the initial value of the pressure taken from the turbulent model atmosphere. Because these integrations, as performed by the Victoria code, do not allow for macroturbulence, the long-dashed curves tend to be close to the dashed curves. In fact, they are so similar in the case of all of the other quantities considered in this figure that the long-dashed curves have not been plotted in the other panels (for the sake of clarity). All of the calculations assume  $\alpha_{\text{MLT}} = 1.77$ , and solar model parameters.

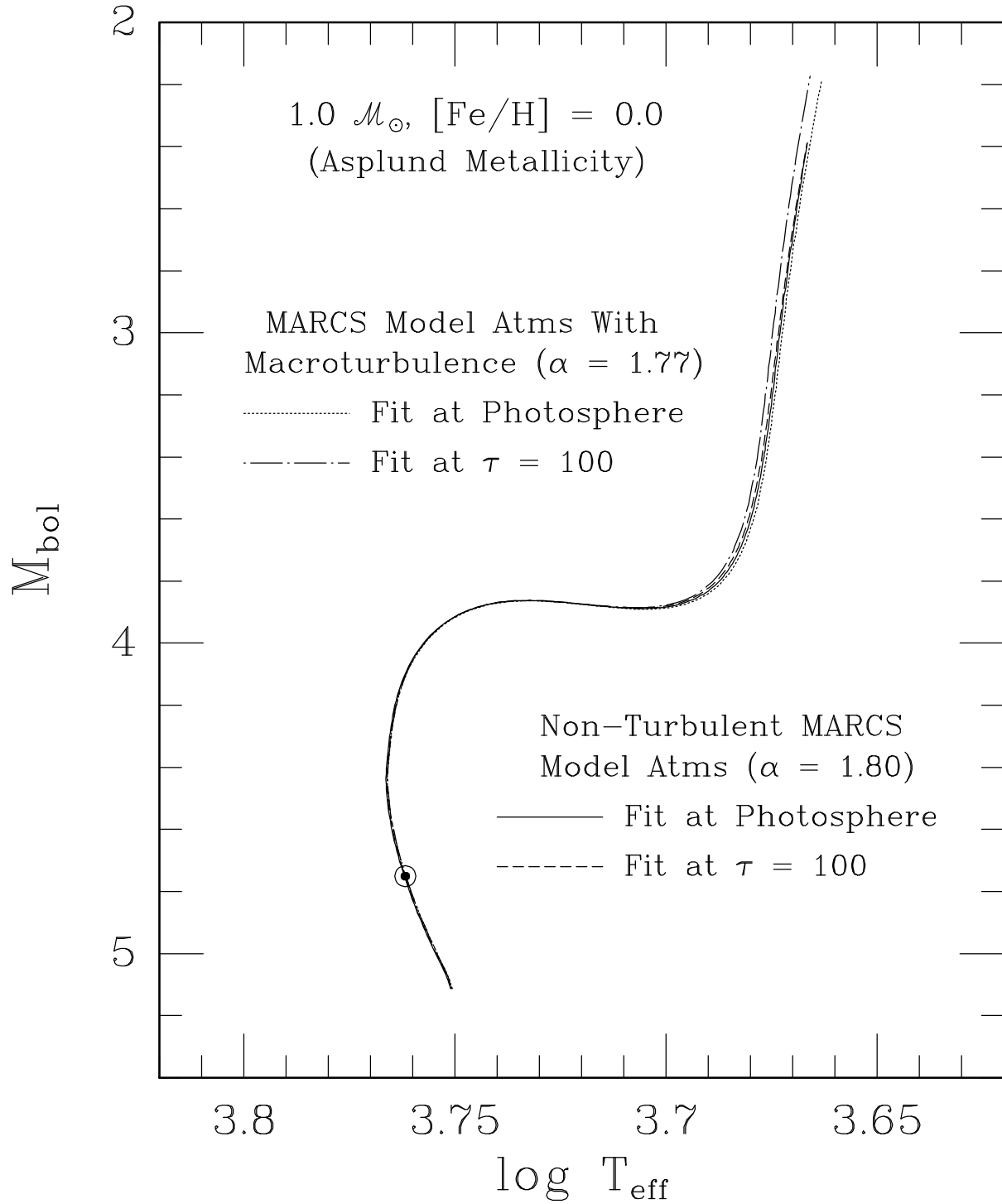


Fig. 10.— Similar to Fig. 3; in this case, evolutionary tracks are compared that use turbulent or non-turbulent MARCS model atmospheres as boundary conditions.

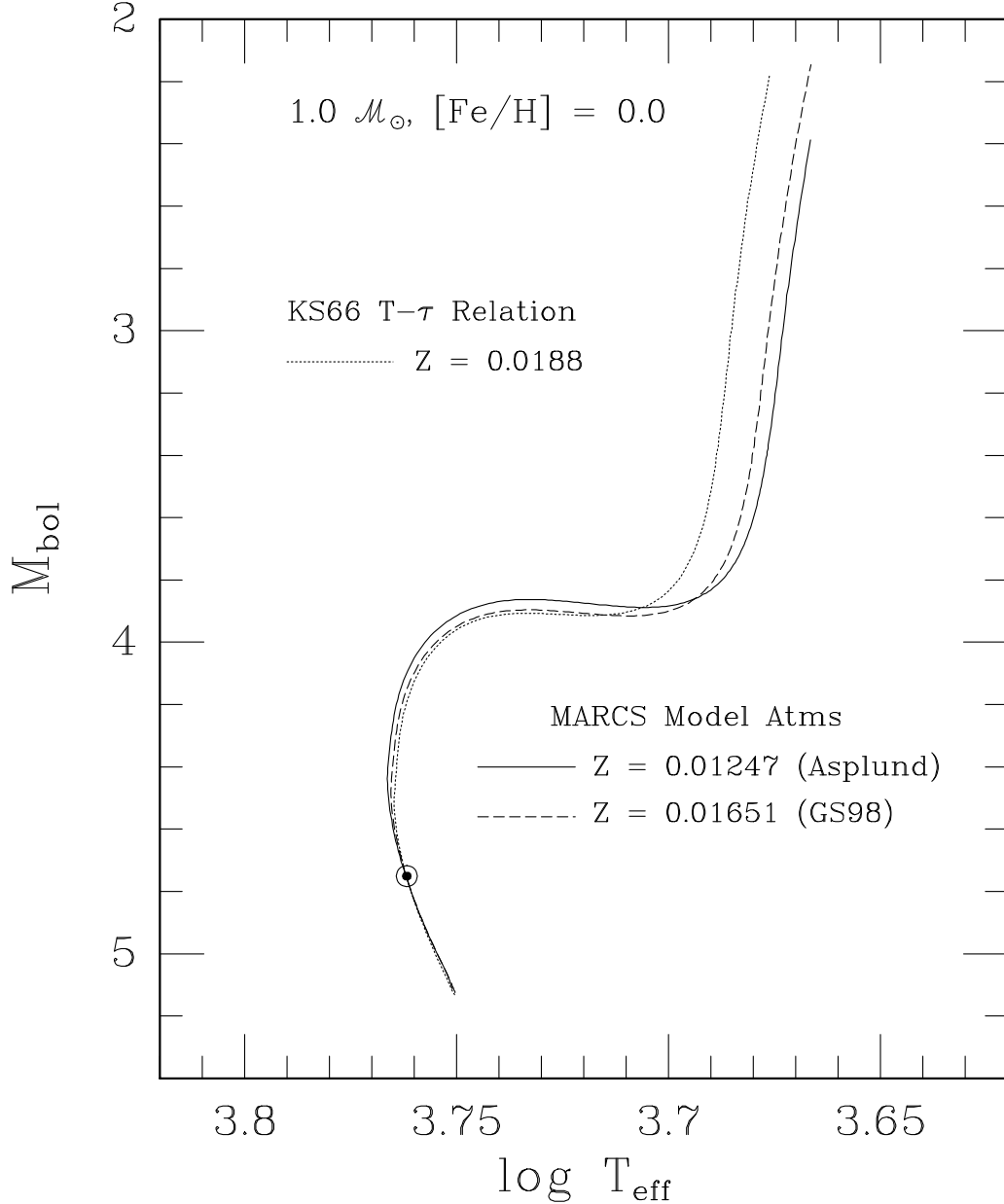


Fig. 11.— Similar to Fig. 3; in this case, the dependence of solar evolutionary tracks on the assumed value of  $Z_{\odot}$  is shown. The solid and dashed curves were computed using boundary conditions derived from non-turbulent MARCS model atmospheres for  $Z_{\odot} = 0.01247$  and  $0.01651$ , on the assumption of the Asplund and GS98 heavy-element mixtures, respectively, and the values of  $Y$  and  $\alpha_{\text{MLT}}$  given in Table 2. They were fitted to the interior models at the photosphere. The dotted curve was taken from the grid of models computed by Vandenberg et al. (2006): it assumes  $Z_{\odot} = 0.0188$  (with the heavy-element mixture given by Grevesse & Noels 1993),  $Y_{\odot} = 0.2715$ , and  $\alpha_{\text{MLT}} = 1.91$ . Boundary pressures for these models were determined using KS66 atmospheric structures.

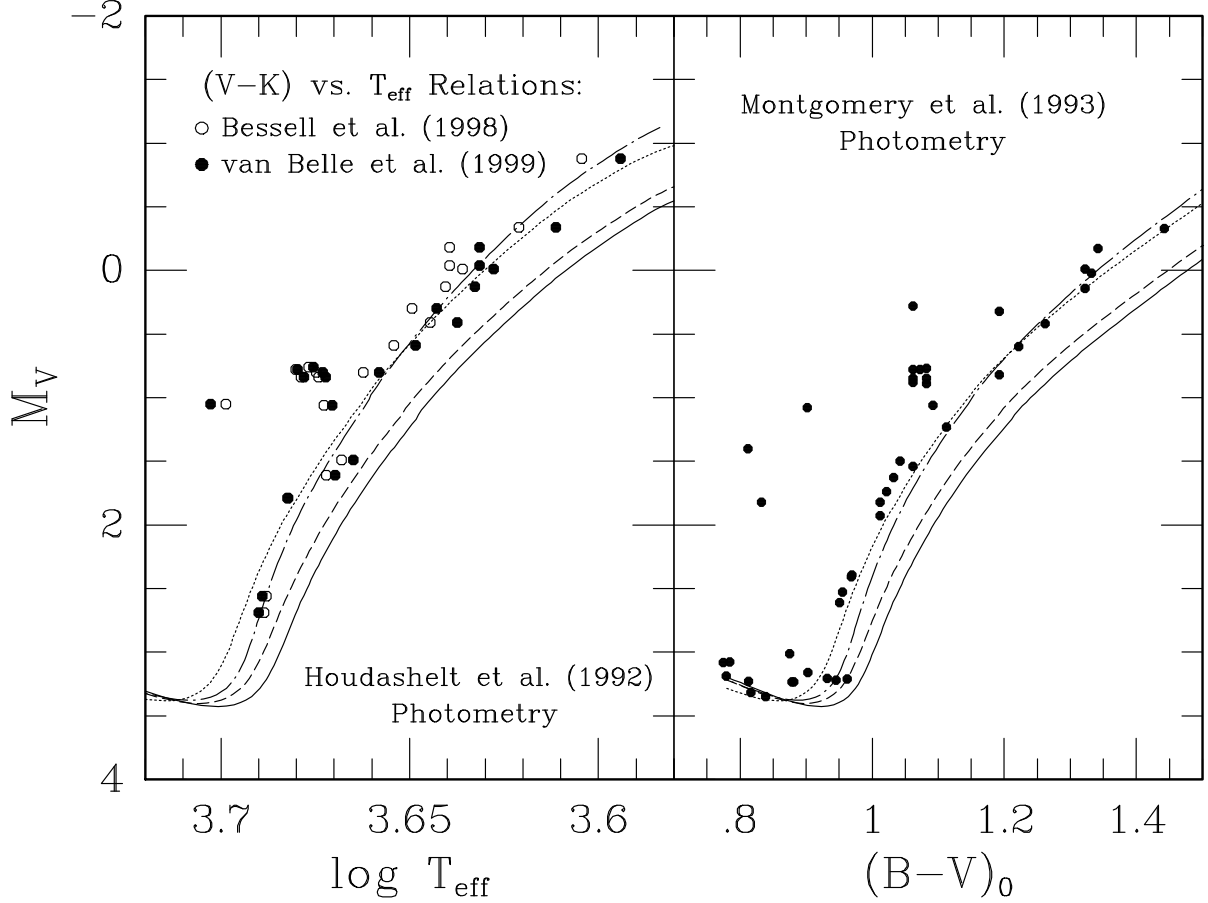


Fig. 12.— *Left-hand panel:* Plot of the M67 giants for which temperatures were derived by applying the empirical  $(V - K) - T_{\text{eff}}$  relations by Bessell et al. (1998; open circles) and van Belle et al. (1999; filled circles) to the  $VK$  photometry by Houdashelt et al. (1992). The assumed  $E(B - V)$  and  $(m - M)_V$  values are 0.038 mag and 9.70 mag, respectively. The dotted curve gives the giant-branch segment of the 4.0 Gyr,  $Z = 0.0173$  isochrone that was used by VandenBerg & Clem (2003) to fit the M67 CMD. The solid and dashed curves represent, in turn, the extensions to high luminosities of the 4.2 Gyr,  $Z = 0.01247$  and 3.9 Gyr,  $Z = 0.01651$  isochrones that were fitted to the CMD of M67 by VandenBerg et al. (2007). The dot-dashed curve represents an otherwise identical calculation to that indicated by the solid curve, except that MARCS SDC model atmospheres were used as boundary conditions (see the text). *Right-hand panel:* As for the left-hand panel, except that the models are compared with the  $BV$  photometry of cluster giants reported by Montgomery et al. (1993).

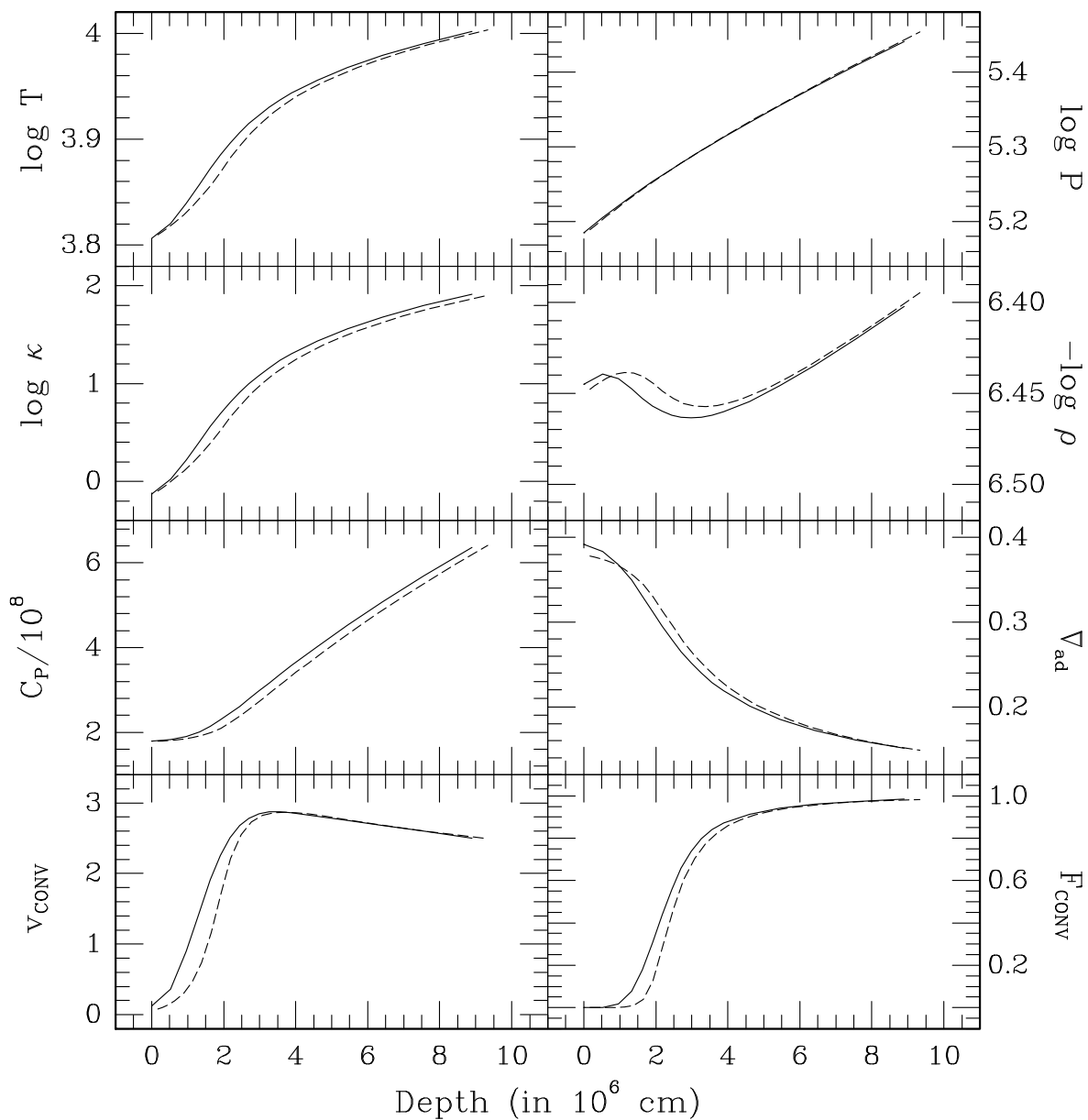


Fig. 13.— Similar to Fig. 1, except that the comparison of the various quantities is made for a model having  $T_{\text{eff}} = 6398$  K,  $\log g = 4.59$ , and  $[\text{Fe}/\text{H}] = -2.0$  (assuming the heavy-element mixture in Table 3).

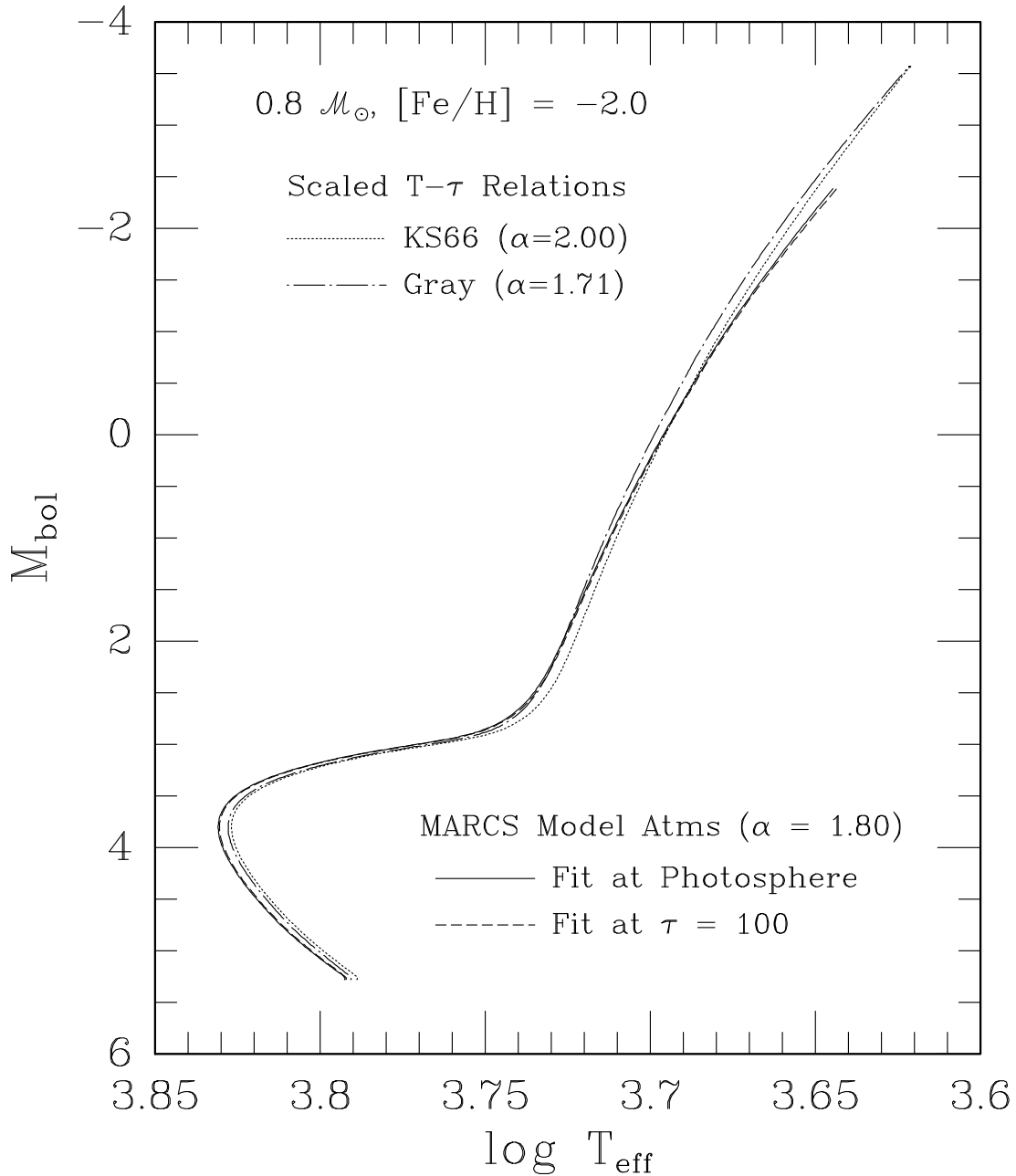


Fig. 14.— Similar to Fig. 3, except that tracks for  $0.8\mathcal{M}_\odot$  stars having  $Y = 0.24823$  and  $Z = 0.00028$  (assuming the heavy-element mixture in Table 3) are plotted. The indicated values of  $\alpha_{\text{MLT}}$  are the same as those required by the corresponding Standard Solar Models. The solid and dashed curves do not extend to the tip of the giant branch because MARCS model atmospheres were not computed for gravities less than  $\log g = 0.0$ .

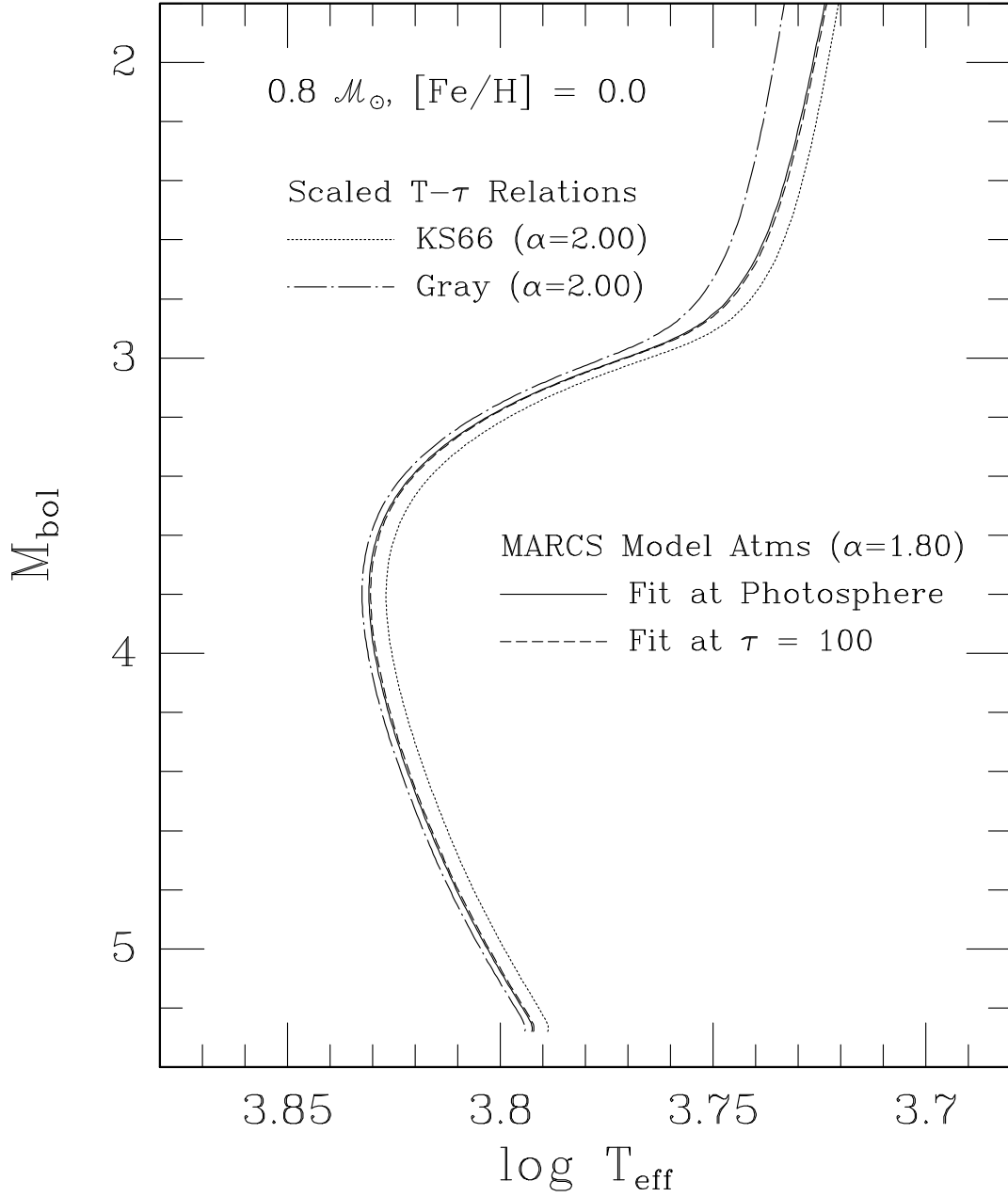


Fig. 15.— An expanded version of the previous plot (to reveal the differences in the vicinity of the turnoff more clearly) in which the track using gray atmospheres has been recomputed on the assumption of  $\alpha_{\text{MLT}} = 2.0$  (instead of 1.71).

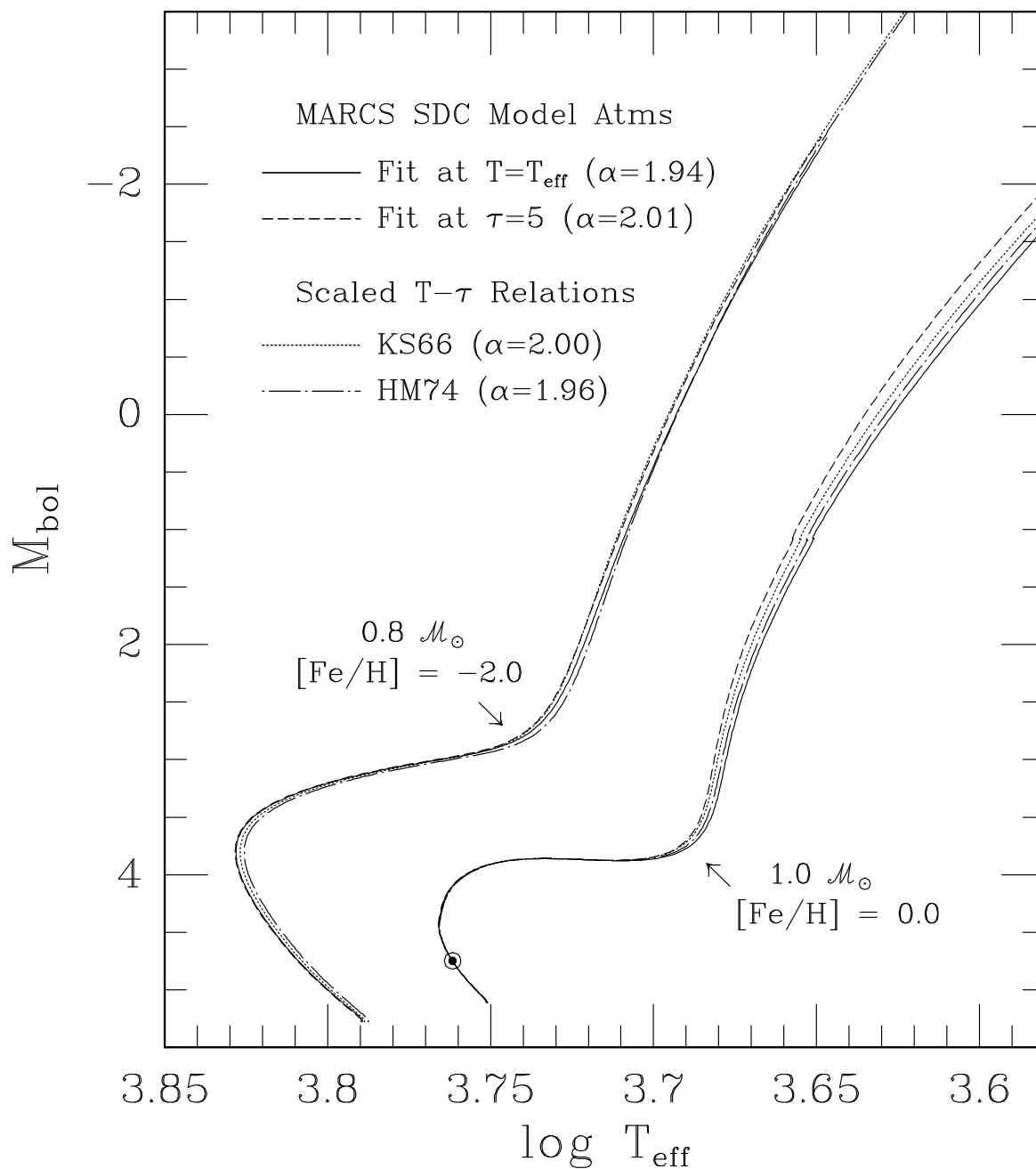


Fig. 16.— Comparisons of the tracks for  $1.0M_{\odot}$ , solar-abundance stars and those for  $0.8M_{\odot}$  stars having  $[\text{Fe}/\text{H}] = -2.0$  when four different treatments of the atmospheric layers are assumed, as indicated. The mixing-length parameter has been set, in each case, to the value required by a Standard Solar Model.

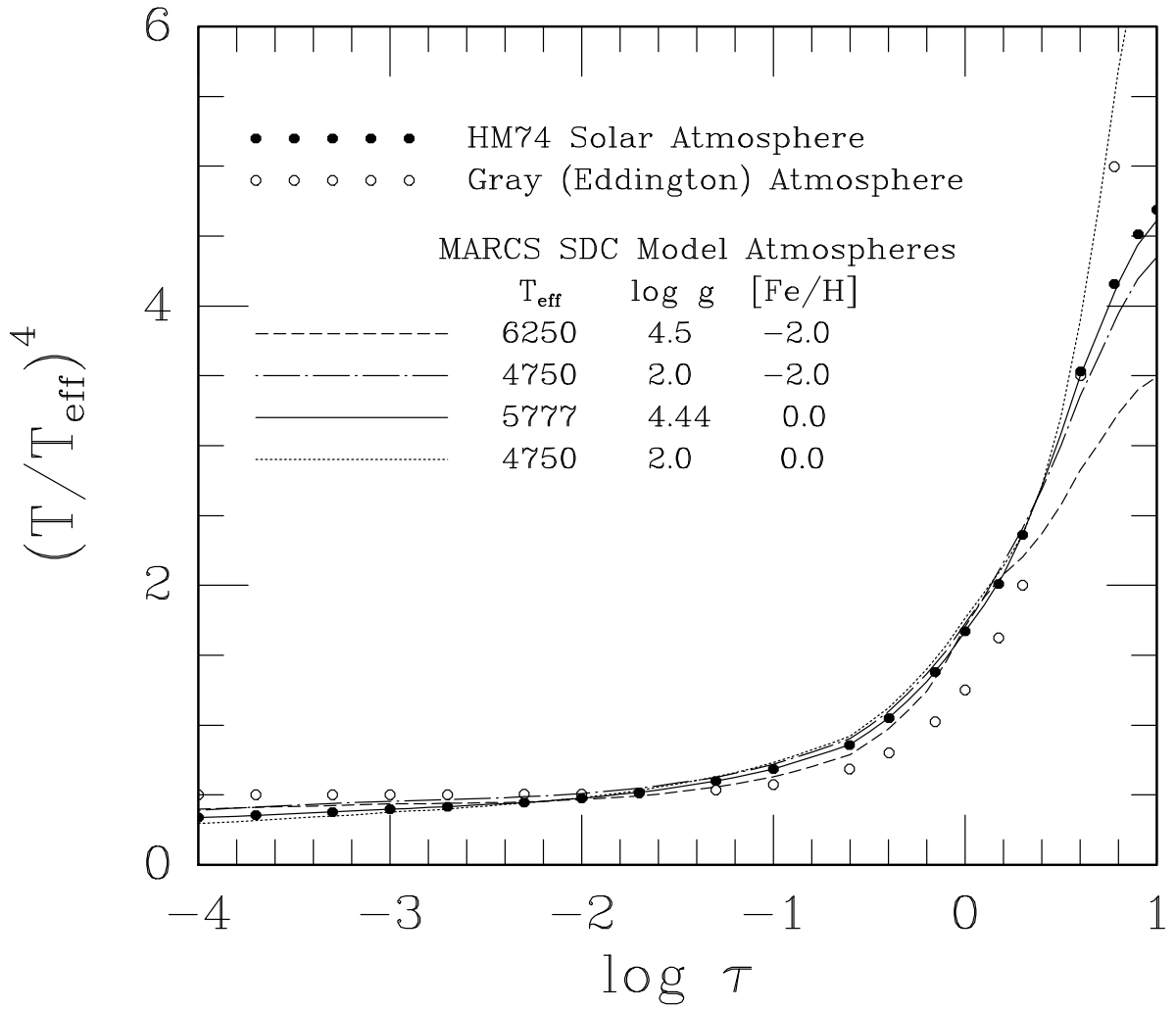


Fig. 17.— Comparison of the scaled  $T$ - $\tau$  structures predicted by MARCS SDC model atmospheres for the indicated parameters with those given by the HM74 and classical gray atmospheres.

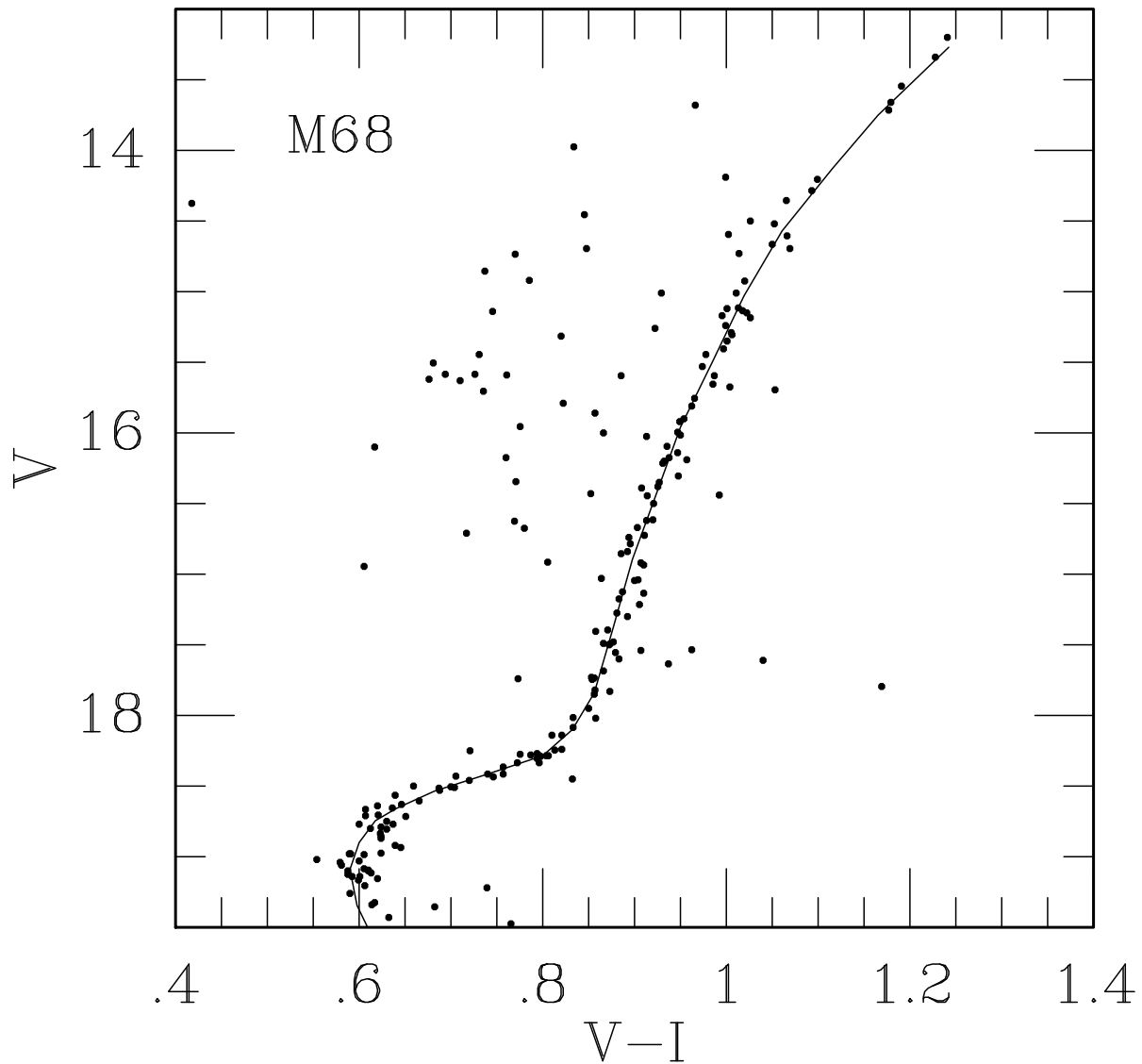


Fig. 18.— Plot of the standard field photometry of the globular cluster M68 provided by Stetson (2000; small filled circles) with the fiducial sequence (solid curve) derived in this investigation to represent the observed CMD for the evolved stars. This merges smoothly into the mean locus for the fainter stars derived by Vandenberg (2000) from the  $VI$  photometry obtained by Walker (1994). The combined fiducial so obtained is used in the following figures.

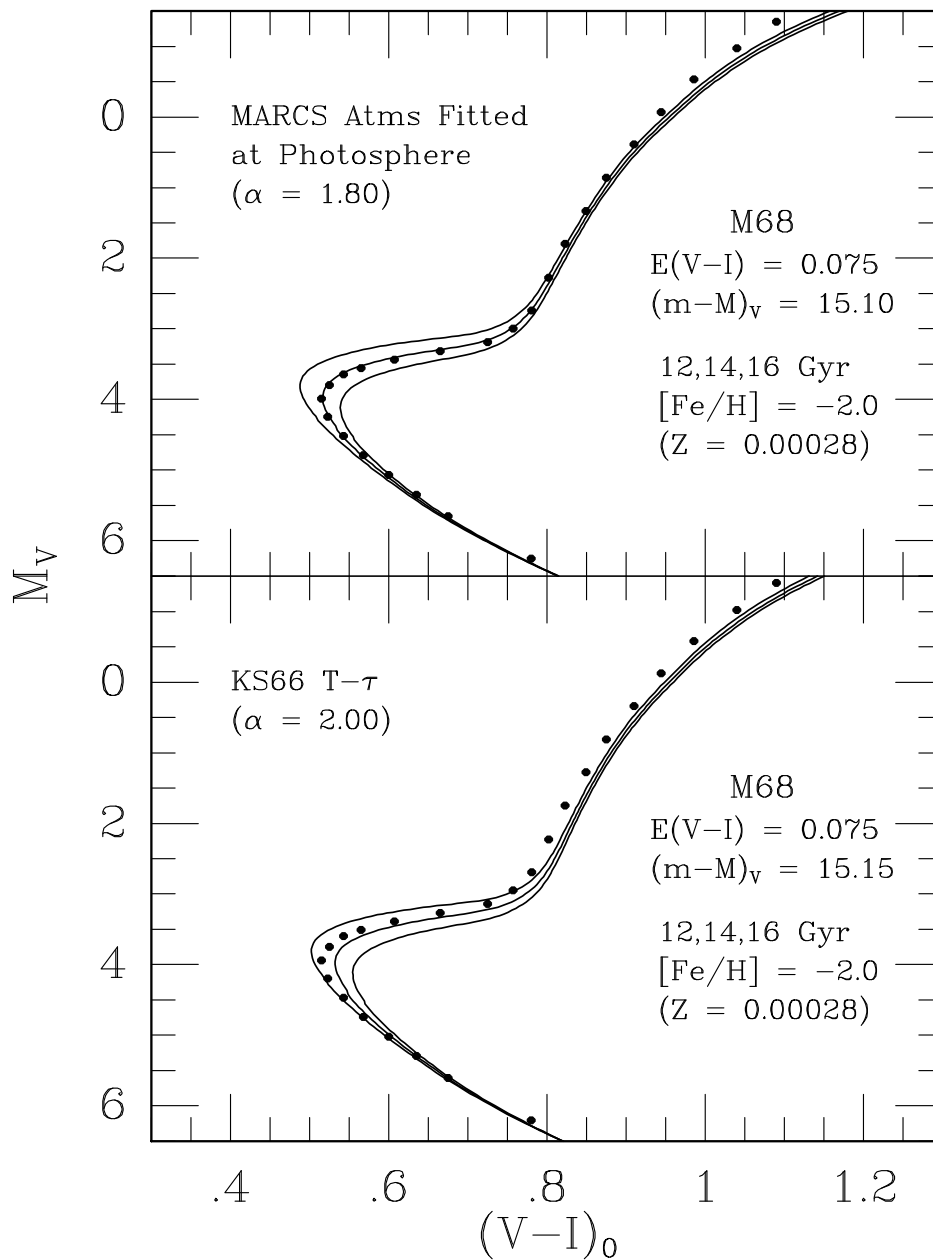


Fig. 19.— Comparisons of isochrones (solid curves) for the indicated ages and chemical abundances with the adopted fiducial sequence of M68 (filled circles). The models used in the upper and lower panels are based on different treatments of the atmosphere and values of  $\alpha_{MLT}$ , as noted. The adopted reddening is from the Schlegel et al. (1998) dust maps, while the indicated distance moduli were derived from main-sequence fits to the isochrones.

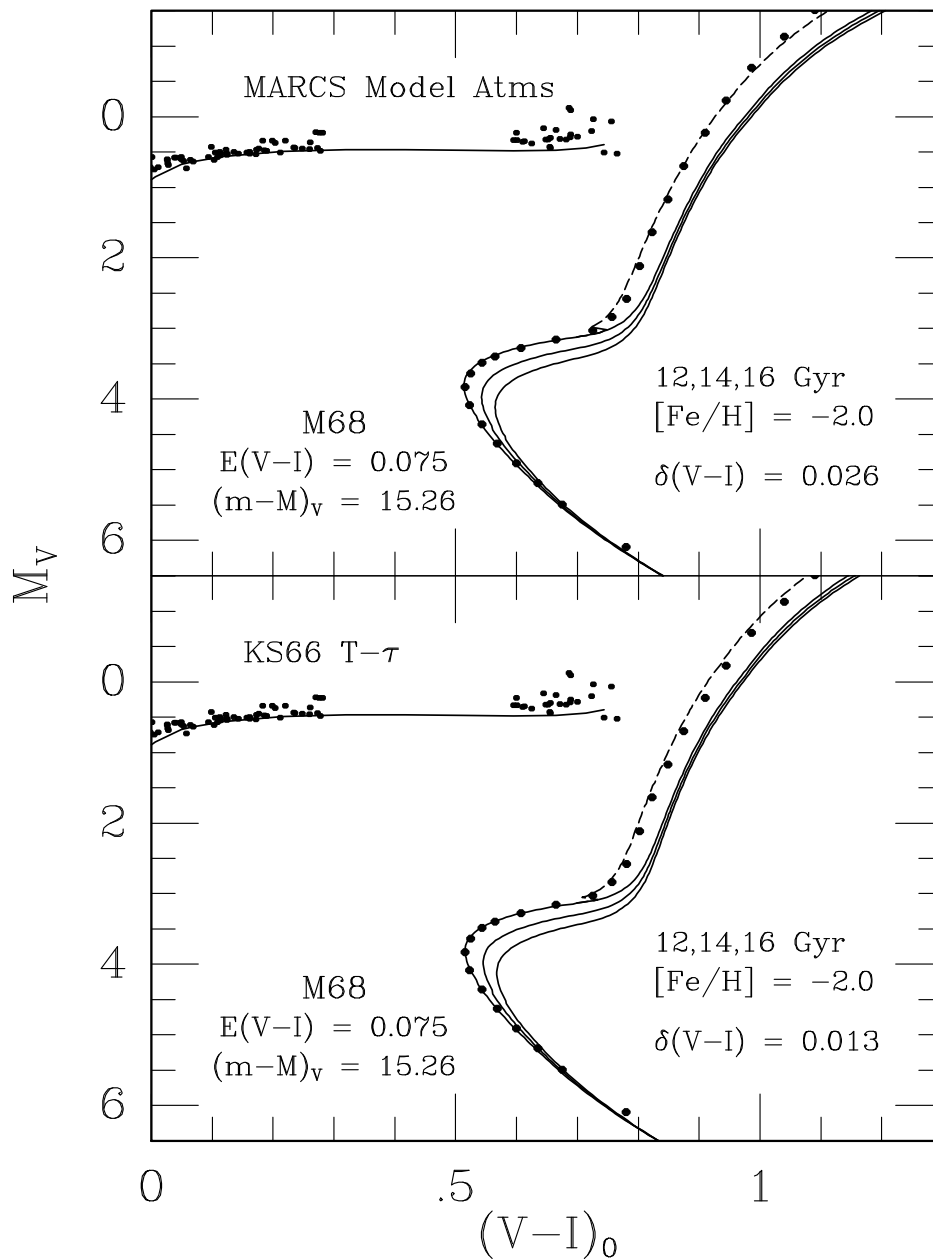


Fig. 20.— Similar to the previous figure, except that the assumed distance is based on a fit of a fully consistent ZAHB to the lower bound of the distribution of the cluster horizontal-branch stars. The source of the HB photometry is Walker (1994). Note that the isochrones had to be shifted to the red, by the indicated amounts, to achieve a superposition of their lower main-sequence segments with the cluster fiducial at  $M_V \gtrsim 5$ .

Table 1. Solar Elemental Abundances

Element	log $N$	
	Grevesse & Sauval (1998)	Asplund <sup>a</sup>
C	8.52	8.41
N	7.92	7.80
O	8.83	8.66
Ne	8.08	7.84
Na	6.33	6.33
Mg	7.58	7.58
Al	6.47	6.47
Si	7.55	7.51
P	5.45	5.45
S	7.33	7.33
Cl	5.50	5.50
Ar	6.40	6.18
K	5.12	5.12
Ca	6.36	6.36
Ti	5.02	5.02
Cr	5.67	5.67
Mn	5.39	5.39
Fe	7.50	7.45
Ni	6.25	6.25
$Z$	0.0165	0.0125

<sup>a</sup>Abundances for C, N, O, Ne, Si, Ar, and Fe were provided by M. Asplund (2004, priv. comm.): Grevesse & Sauval (1998) abundances are assumed for all other elements heavier than helium. ( $\log N_{\text{H}} \equiv 12.00$ .)

Table 2. Parameters of Standard Solar Models

Metals Mixture	$\alpha_{\text{MLT}}^{\text{a}}$	$\log N_{\text{He}}$	$X$	$Y$	$Z$
Grevesse & Sauval (1998)	1.84	10.9738	0.71585	0.26764	0.01651
Asplund (see Table 1)	1.80	10.9487	0.72995	0.25758	0.01247

<sup>a</sup>Obtained when MARCS non-turbulent model atmospheres are attached to the interior structures at  $T = T_{\text{eff}}$ .

Table 3. Adopted Abundances at  $[\text{Fe}/\text{H}] = -2$

Element	$\log N$	$[\text{m}/\text{H}]$	$[\text{m}/\text{Fe}]$
C	6.41	-2.0	0.0
N	5.80	-2.0	0.0
O	7.16	-1.5	+0.5
Ne	6.14	-1.7	+0.3
Na	4.03	-2.3	-0.3
Mg	5.88	-1.7	+0.3
Al	4.47	-2.0	0.0
Si	5.91	-1.6	+0.4
P	3.45	-2.0	0.0
S	5.63	-1.7	+0.3
Cl	3.50	-2.0	0.0
Ar	4.48	-1.7	+0.3
Ca	4.66	-1.7	+0.3
Ti	3.22	-1.8	+0.2
Cr	3.27	-2.4	-0.4
Mn	2.99	-2.4	-0.4
Fe	4.45	-2.0	0.0
Ni	4.25	-2.0	0.0